Thesis

Exploring the brain's microstructure by using diffusion spectrum imaging and double diffusion encoding magnetic resonance imaging

（拡散スペクトラムイメージングとダブル拡散エンコーディング磁気共鳴画像を用いた脳の微細構造の評価）

March 2022

Hokkaido University

Xinnan Li

Table of contents

Presented paper list and conference presentation list

Part of this study was presented in the following papers:

Li, X., Sawamura, D., Hamaguchi, H., Urushibata, Y., Feiweier, T., Ogawa, K. Tha, K.K. (2022). Microscopic Fractional Anisotropy Detects Cognitive Training-Induced Microstructural Brain Changes. Tomography 8, 33-44.

Part of this study was presented in the following academic conferences:

1. Li, X., Abiko, K., Urushibata, Y., Hamaguchi, H., Ahn, S., Tha, K.K. Microstructural Attributes of Hemispheric Lateralization: A Combined Evaluation of Diffusion Spectrum Imaging and MR Spectroscopic Imaging. International Society for Magnetic Resonance in Medicine Virtual Conference & Exhibition, August 2020 (Virtual).
2. Li, X., Sawamura, D., Hamaguchi, H., Urushibata, Y., Feiweier, T., Ogawa, K., Tha, K.K. Tissue Microstructural Changes following Four-Week Neurocognitive Training: Observations of Double Diffusion Encoding MRI. International Society for Magnetic Resonance in Medicine Virtual Conference & Exhibition, May 2021 (Virtual).

Abbreviation table

3D	3-dimensional
ANOVA	analysis of variance
ANT	attention network training
ATP	adenosine triphosphate
Cho	choline
Cr	creatine
CSF	cerebrospinal fluid
DBT	dual N-back training
DDE	double diffusion encoding
DTI	diffusion tensor imaging
DSI	diffusion spectrum imaging
DWI	diffusion-weighted imaging
FLAIR	fluid-attenuated inversion recovery
FOV	field of view
FA	fractional anisotropy
fMRI	functional MRI
FWHM	full width at half maximum
GFA	generalized fractional anisotropy
Glx	glutamate and glutamine compounds
LI	laterality index
MD	mean diffusivity
mI	myoinositol
μFA	microscopic fractional anisotropy
MIDAS	Metabolic Imaging and Data Analysis System
MNI	Montreal Neurological Institute
MPRAGE	magnetization-prepared rapid acquisition gradient echo

MRI	magnetic resonance imaging
MRS	magnetic resonance spectroscopy
NAA	N-acetyl aspartate
NEX	number of excitation
NQA	normalized quantitative anisotropy
ODF	orientation distribution function
PDWI	proton density-weighted imaging
ROI	region of interest
RT	response time
SD	standard deviation
SNR	signal-to-noise ratio
SPM	statistical parametric mapping
SPSS	statistical package for the social sciences
TA	acquisition time
TE	echo time
TI	inversion time
TR	repetition time
WB-MRSI	whole-brain magnetic resonance spectroscopic imaging

Introduction

Magnetic resonance imaging (MRI) is a non-invasive imaging technique that has been widely used to study brain morphology and function in normal and pathological states. The main advantages of MRI over other imaging techniques are high spatial resolution, superb tissue contrast, and no radiation exposure. Of several MRI techniques, diffusion MRI can provide information about the cellular environment of the brain and characterize brain tissue microstructure by detecting the diffusion of water molecules that is not possible with conventional MRI techniques. Diffusion-weighted imaging (DWI) is the most frequently used and fundamental diffusion MRI sequence. Following the invention of DWI, several diffusion MRI techniques that provide more detailed information about the biological tissue environment have been developed.

Diffusion tensor imaging (DTI) is one of the modifications of diffusion MRI. It is a useful tool to illustrate the microstructural brain changes in various pathological states such as brain tumors, acute stroke, abscess, multiple system atrophy, and major depressive disorder (Kono et al., 2001; Lansberg et al., 2000; Leuthardt et al., 2002; Tha et al., 2010, 2013). It employs a tensor model that consists of three principal orthogonal eigenvectors to evaluate the white matter microstructure. In white matter fibers, diffusion in the principal direction of fibers is faster than that in the perpendicular direction. Such variation in the rate of water diffusion in different directions is termed anisotropy (Fujiyoshi et al., 2013), which can be quantified by a DTI index termed fractional anisotropy (FA). FA ranges from 0 (isotropic diffusion) to 1 (anisotropic diffusion). Decreased FA in white matter fibers is considered to reflect the reduced white matter integrity due to neuronal and volume loss, axonal degeneration, demyelination, etc (Budde et al., 2011). Mean diffusivity (MD) is another DTI index, which quantifies the magnitude of diffusion of water molecules. The faster the diffusion, the greater is the MD. Although DTI has been widely used to evaluate the white matter microstructure in normal and pathological states, drawbacks of DTI have been reported. Because DTI tracks white matter fibers based on the principal orientations, the anisotropy values of all fiber orientations in the same voxel are the same. This fails DTI to resolve anisotropic structures aligned in several

orientations, such as dispersing or crossing white matter fibers (Lasič et al., 2014).

To overcome the drawbacks of DTI, several advanced diffusion MRI techniques have been developed. Of these techniques, diffusion spectrum imaging (DSI) is a model-free method, which can display crossing fibers and complex intravoxel fiber orientation distributions reliably and accurately (Wedeen et al., 2008). The angular resolution to model a 3-dimensional (3D) orientation distribution function (ODF) has been reported as satisfactory (Wedeen et al., 2005). DSI is also reported to have higher sensitivity in detecting crossing fibers than the other diffusion MRI techniques such as DTI, diffusional kurtosis imaging, and q-ball imaging (Glenn et al., 2016; Kuo et al., 2008). This high sensitivity of DSI is achieved through the use of higher b values and hundreds of sampling directions (Wedeen et al., 2005). Thus, a high gradient performance MRI system and long scan time are required to acquire DSI. With the recent development of rapid acquisition techniques, the scanning time of DSI has been reduced from 50 to 17 min while retaining high image quality. This allows the clinical applicability of this technique (Bilgic et al., 2012). For a better understanding of changes in DSI indices in pathological states, the regional normative values would be necessary. Diffusion indices such as FA and MD of DTI are known to vary with anatomical location, gender, and age (Bhagat and Beaulieu, 2004; Huster et al., 2009; Panesar et al., 2017). Regional normative values of DSI indices are not known. Chapter 1 of this thesis reports the normative values of DSI indices in the whole brain and their variations of anatomical location, gender, and age. Hemispheric lateralization of these indices and their relationship with neurometabolites are reported in Chapter 2.

The drawbacks of DTI can also be resolved by employing multiple diffusion encoding schemes such as double diffusion encoding (DDE) MRI. These diffusion schemes are possible with recent improvements in gradient systems of clinical scanners. Compared to DTI that uses only a single diffusion gradient pair, DDE MRI applies two diffusion gradient pairs in parallel and orthogonal directions, which can improve the sensitivity of obtaining microstructural information by quantifying diffusion anisotropy without the influence of orientation dispersion (Mitra, 1995; Ozarslan, 2009). The major diffusion index derived from DDE MRI is

microscopic fractional anisotropy (μFA). The superiority of μFA over FA of DTI in characterizing anisotropic structures has been reported. Higher resolution in detecting orientation dispersion in μFA over FA was observed in liquid crystal/yeast and pureed asparagus phantom studies (Lasič et al., 2014). The superiority of μFA over FA in distinguishing white matter lesions in the brain has also been reported in patients with multiple sclerosis and Parkinson's disease (Kamiya et al., 2020; Yang et al., 2018). In Chapter 3, whether μFA can identify neuroplastic changes following cognitive training was evaluated.

Chapter 1.

Normative values of diffusion spectrum imaging indices of the brain in adults

1. Introduction

DSI is an advanced diffusion imaging technique that quantifies diffusion orientation distribution function (ODF) by using a Fourier transform relationship between the diffusion signal and the average particle displacement probability density function (Wedeen et al., 2008). The major diffusion indices derived from DSI include generalized fractional anisotropy (GFA) and normalized quantitative anisotropy (NQA). GFA is the equivalent index to the FA of DTI and represents the probability distribution of the diffusion displacement (Tuch, 2004). NQA is a normalized index of quantitative anisotropy and represents a quantitative distribution of the spins undergoing diffusion (Yeh, Wedeen, and Tseng, 2010). DSI is a model-free method to characterize the brain microstructure, and considered as can accurately capture restricted diffusion. The superiority of DSI over DTI in resolving intravoxel fiber crossing issues has been reported in diffusion ODF reconstruction and white matter tractography (Glenn et al., 2016).

In general, determination on whether there is any alteration in the diffusion indices in a given voxel or region-of-interest is done by comparing the local values with the normative reference values. Thus, knowledge about normative values of diffusion indices and their variations with age, gender, and anatomical location is essential. A previous DSI study that evaluated the influence of age on GFA in the corpus callosum has reported its decrease with age in the anterior part of the structure (Teipel et al., 2014). Whether there is an age-related variation of the DSI indices in other anatomical locations is not known. Similarly, it is not known whether these indices vary with anatomical location and gender. According to previous DTI studies, FA and MD vary with anatomical location, gender, and age. For example, FA is higher in the corpus callosum and lower in the deep gray matter nuclei and cerebellar vermis (Panesar et al., 2017). Men have higher FA and lower MD in the cingulum than women (Huster et al., 2009). In addition, FA increases with age in the putamen and decreases in sublobar white matter (i.e. corpus callosum and internal and external capsule), frontal, temporal, and occipital

gyri (Bhagat and Beaulieu, 2004). Considering these variations and that DSI is a modified diffusion imaging sequence, anatomical location-, age-, and gender-related variations in GFA and NQA may exist.

This prospective study aimed to determine the normative values of the major DSI indices across the brain in adults and their variation with anatomical locations, age, and gender.

2. Materials and methods

2.1. Participants

This prospective study was approved by the institutional review board of Hokkaido University. Written informed consent was obtained from all participants. Volunteers were recruited over a recruitment period of 21 months (2016/07 ~ 2018/03). The inclusion criterion was aged from 20 to 65 years old. The exclusion criteria included absolute contraindications for MRI, history of diseases that might affect the integrity of the central nervous system, gross abnormalities on conventional MR images {i.e., fluid-attenuated inversion recovery (FLAIR) imaging sequences}, and visible motion artifacts on DSI dataset. Of 39 volunteers who consented to the study, three volunteers were excluded because of motion artifact. This resulted in a total of 36 healthy participants {17 women and 19 men; age range = 22 - 60 years, mean age ± standard deviation (SD) = 34.56 ± 10.74 years}.

2.2. MRI

MRI was performed using a 3T scanner (MAGNETOM Prisma, Siemens Healthcare, Erlangen, Germany) and a 64-channel head/neck coil.

DSI was acquired using a spin-echo echo-planar sequence (repetition time (TR)/echo time (TE) = 4000 ms/100 ms, flip angle = 90°, field of view (FOV) = 240 × 240 mm^2, matrix = 96 × 96, voxel size = 2.5 × 2.5 × 2.5 mm^3, 128 isotropically distributed diffusion-weighted directions, maximum b-value = 8000 s/mm^2, q-space weightings = 5, multiband factor = 2, acquisition time (TA) = 17:52 min). In addition, T1-weighted 3-dimensional (3D) magnetization-prepared rapid acquisition gradient echo (MPRAGE) sequence

(TR/TE/inversion time (TI) = 1900 ms/2.85 ms/900 ms, flip angle = 9°, voxel size = 0.9 × 0.9 × 0.9 mm^3, FOV = 230 × 230 mm^2, matrix = 256 × 256, number of excitation (NEX) = 1, TA = 4:50 min) was acquired for anatomical information, tissue segmentation, spatial normalization of the reconstructed maps. Axial FLAIR imaging sequence (TR/TE/TI = 12000 ms/115 ms/2800 ms, flip angle = 150°, slice thickness = 5 mm, FOV = 199 × 220 mm^2, matrix = 203 × 320, NEX = 1, TA = 2:24 min) and axial proton density-weighted imaging (PDWI) sequence (TR/TE = 4000/12 ms, flip angle = 160°, slice thickness = 3 mm, FOV = 220 × 220 mm^2, matrix = 320 × 240, NEX = 1, TA = 3:08 min) were also acquired to exclude gross abnormalities and white matter hyperintensities. Review of conventional MR imaging sequences and diffusion images to exclude any abnormalities and artifacts was done by a radiologist with 19-year experience in neuroimaging.

2.3. Data processing

2.3.1. Reconstruction of maps of DSI indices

GFA and NQA maps were reconstructed from the DSI data, using DSI studio software package version Mar 15 2016 (http://dsi-studio.labsolver.org) (Yeh, Wedeen, and Tseng, 2010). Maps of two major DTI indices, FA and MD, were also reconstructed for comparison. Default processing parameters were applied. GFA was calculated as the division of the SD and root mean square of the ODF value (Tuch, 2004). NQA was calculated as the spin distribution function value (i.e. ODF multiplied by the spin density) at the restricted fiber orientation minus the background isotropic diffusion component (Yeh, Wedeen, and Tseng, 2010). FA was calculated as the division of the SD of eigenvalues of the diffusion tensor and their root mean square, and MD was defined as the average of eigenvalues of the diffusion tensor (Pierpaoli and Basser, 1996).

2.3.2. Spatial normalization

The MPRAGE images were spatially normalized to the standard Montreal Neurological Institute (MNI) space. The transformation parameters were then applied to the corresponding

co-registered GFA, NQA, FA, and MD maps, by using Statistical Parametric Mapping 12 (SPM12) software (Wellcome Trust Centre for Neuroimaging, London, UK), which runs on MATLAB version 7.9.0 R2009b (The MathWorks, Natick, Massachusetts, USA). Default parameters of SPM12 were used.

2.3.3. Generation of brain mask

After generating the spatially normalized maps, voxels other than the brain tissues in the spatially-normalized GFA, NQA, FA, and MD maps were removed by applying a brain parenchyma mask. This brain mask was generated by segmenting the brain tissues (gray and white matter) voxels from the corresponding spatially normalized mean MPRAGE images derived from all participants (SPM12). Then, the brain mask was allowed to dilate for a single voxel to reduce the influence of partial volume errors, using ImageJ software version 1.51 (National Institutes of Health, Bethesda, MD, USA) (Schneider, Rasband, and Eliceiri, 2012).

2.3.4. Placement of regions-of-interest

Fourteen anatomical regions of interest (ROIs) almost covers the whole brain, including frontal, parietal, temporal, occipital, insular and limbic lobes, caudate and lentiform nuclei, claustrum, thalamus, sublobar white matter (containing corpus callosum, external and internal capsules, and periventricular white matter), midbrain, pons, and cerebellar hemispheres, were selected from the Wake Forest University PickAtlas toolbox version 3.0.5 (Wake Forest University School of Medicine, Winston-Salem, USA) (Maldjian et al., 2003). The exact anatomical location of each ROI is given in Figure 1. These ROIs were then applied onto the normalized GFA, NQA, FA, and MD maps to extract the mean values.

Figure 1. The outline of the regions of interest (ROIs), including frontal, parietal, temporal, occipital, insular and limbic lobes, caudate and lentiform nuclei, claustrum, thalami, sublobar white matter (corpus callosum, external and internal capsules, and periventricular white matter), midbrain, pons, and cerebellum, overlaid on the axial sections of normalized T1-weighted 3-dimensional (3D) magnetization-prepared rapid acquisition gradient echo (MPRAGE) images. L and R indicate left and right, respectively.

2.4. Statistical analysis

Variations in GFA, NQA, FA, and MD among anatomical locations were evaluated by using repeated-measures analysis of variance (ANOVA) with post-hoc Bonferroni analyses. Variations in these indices between the gender groups were evaluated by using two sample t-tests. The correlation of these indices with age was evaluated by using Pearson's product-moment correlation analyses. Age and gender were considered as covariates whenever appropriate. For all analyses, $P < 0.05$ after correction for multiple comparisons was considered significant. All statistical analyses were performed using Statistical Package for the Social Sciences (SPSS) software version 22 (IBM, New York, USA).

3. Results

The representative maps are shown in Figure 2.

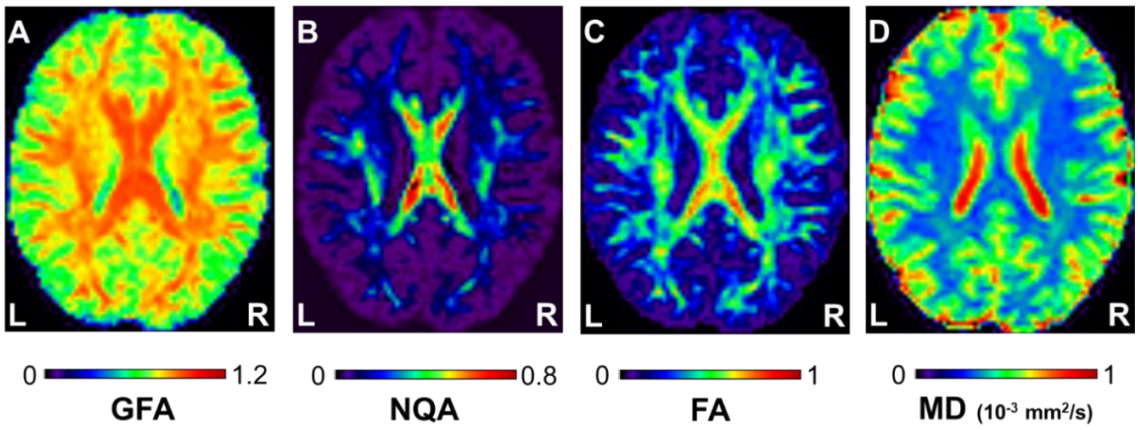

Figure 2. Maps of the diffusion indices of a 25-year man. (A) generalized fractional anisotropy (GFA), (B) normalized quantitative anisotropy (NQA), (C) fractional anisotropy (FA), and (D) mean diffusivity (MD). The lookup table indicates the value of each index. L and R indicate left and right, respectively.

3.1. Variation in the DSI indices with anatomical location

The mean regional GFA and NQA, along with FA and MD, are provided in Table 1.

GFA, NQA, and FA exhibited a similar pattern of regional distribution. In summary, the pons had the highest GFA, NQA, and FA. The other white matter areas (i.e. midbrain and sublobar area) had significantly higher GFA, NQA, and FA than the other anatomical locations (corrected $P < 0.011$). Among major cerebral lobes (i.e. frontal, parietal, temporal, and occipital lobes), the frontal lobe had significantly higher and the occipital lobe had significantly lower GFA, NQA, and FA (corrected $P < 0.001$). Among deep gray matter nuclei, the lentiform nucleus had significantly higher and the caudate nucleus had significantly lower GFA, NQA, and FA (corrected $P < 0.001$). The limbic lobe had significantly higher GFA and NQA than the insular lobe (corrected $P < 0.001$), but not FA. The occipital lobe had the lowest GFA and the caudate nucleus had the lowest NQA and FA. The cerebellum had significantly lower GFA, NQA, and FA than most other anatomical locations (corrected $P < 0.010$).

Regarding the regional variation in MD, the caudate nucleus and pons had the highest and

lowest MD, respectively. The white matter areas and lentiform nucleus had significantly lower MD than most other anatomical locations (corrected $P < 0.001$). Among the major cerebral lobes, the frontal lobe had significantly lower MD than the other lobes (corrected $P < 0.001$). The cerebellum had significantly lower MD than the major cerebral lobes (corrected $P < 0.001$). The caudate nucleus had significantly higher MD than most anatomical locations (corrected $P < 0.014$).

Table 1. The mean regional diffusion indices of anatomical regions.

Anatomical location	GFA	NQA	FA	MD (10^{-3} mm^2/s)
Frontal lobe	0.798 ± 0.007 (●)	0.093 ± 0.011 (●)	0.256 ± 0.011 (3~14)	0.397 ± 0.010 (●)
Parietal lobe	0.780 ± 0.010 (1,4~10,12,13)	0.082 ± 0.011 (●)	0.254 ± 0.014 (3~14)	0.429 ± 0.011 (1,5~10,12~14)
Temporal lobe	0.782 ± 0.008 (1,4~10,12,13)	0.076 ± 0.009 (●)	0.240 ± 0.015 (1,2,4,6,8~14)	0.428 ± 0.010 (1,5~10,12~14)
Occipital lobe	0.771 ± 0.009 (●)	0.070 ± 0.008 (●)	0.225 ± 0.013 (1~3,8~14)	0.426 ± 0.010 (1,6~14)
Insula	0.792 ± 0.008 (●)	0.088 ± 0.011 (1~4,6~8,10~13)	0.231 ± 0.018 (1,2,8~14)	0.418 ± 0.012 (1~3,7~14)
Limbic lobe	0.801 ± 0.006 (1~5,7,8,10~14)	0.108 ± 0.013 (●)	0.225 ± 0.012 (1~3,8~14)	0.411 ± 0.008 (1~4,7~14)
Lentiform nucleus	0.821 ± 0.005 (1~6,9~14)	0.117 ± 0.014 (1~6,9~14)	0.226 ± 0.021 (1,2,8~14)	0.352 ± 0.013 (1~6,8,9,11~14)
Claustrum	0.817 ± 0.010 (1~6,9~14)	0.119 ± 0.018 (1~6,9~14)	0.292 ± 0.021 (●)	0.382 ± 0.012 (●)
Thalamus	0.804 ± 0.004 (1~5, 7,8,10~14)	0.089 ± 0.012 (1~4,6~8,10~13)	0.192 ± 0.016 (●)	0.368 ± 0.013 (1~8,10~13)
Sublobar white matter	0.835 ± 0.005 (●)	0.171 ± 0.020 (1~9,11,13,14)	0.358 ± 0.017 (●)	0.357 ± 0.009 (1~6,8~14)
Caudate nucleus	0.783 ± 0.009 (1,4~10,12,13)	0.065 ± 0.009 (●)	0.118 ± 0.010 (●)	0.436 ± 0.018 (1,4~10,12~14)
Midbrain	0.831 ± 0.004 (●)	0.169 ± 0.017 (1~9,11,13,14)	0.325 ± 0.020 (●)	0.318 ± 0.011 (●)
Pons	0.849 ± 0.004 (●)	0.226 ± 0.026 (●)	0.369 ± 0.024 (●)	0.305 ± 0.009 (●)
Cerebellum	0.782 ± 0.007 (1,4~10,12,13)	0.088 ± 0.010 (1~4,6~8,10~13)	0.167 ± 0.010 (●)	0.375 ± 0.008 (1~8,10~13)

Note: The numbers (1~14) and ● in parentheses indicate statistically significant difference with other anatomical locations ($P < 0.05$ following correction for multiple comparisons). In particular, superscript (1,2) indicates statistically significant difference with frontal and parietal lobes, and superscript (●) indicates statistically significant difference with all other anatomical locations. 1 = frontal lobe, 2 = parietal lobe, 3 = temporal lobe, 4 = occipital lobe, 5 = insula, 6 = limbic lobe, 7 = lentiform nucleus, 8 = claustrum, 9 = thalamus, 10 = sublobar white matter, 11 = caudate nucleus, 12 = midbrain, 13 = pons, 14 = cerebellum, ● = all other anatomical locations, GFA = generalized fractional anisotropy, NQA = normalized quantitative anisotropy, FA = fractional anisotropy, MD = mean diffusivity

3.2. Gender variation in DSI indices

Figure 3 illustrates the mean regional diffusion indices in each gender group.

Men had significant higher GFA in the thalamus (corrected P = 0.022), midbrain (corrected P = 0.018), and cerebellum (corrected P = 0.016) than women. On the contrary, women had significantly higher FA in the thalamus (corrected P = 0.031), midbrain (corrected P = 0.018), and pons (corrected P < 0.001), and higher MD in the limbic lobe (corrected P = 0.035), thalamus (corrected P = 0.009), midbrain (corrected P < 0.001), and pons (corrected P < 0.001), than men.

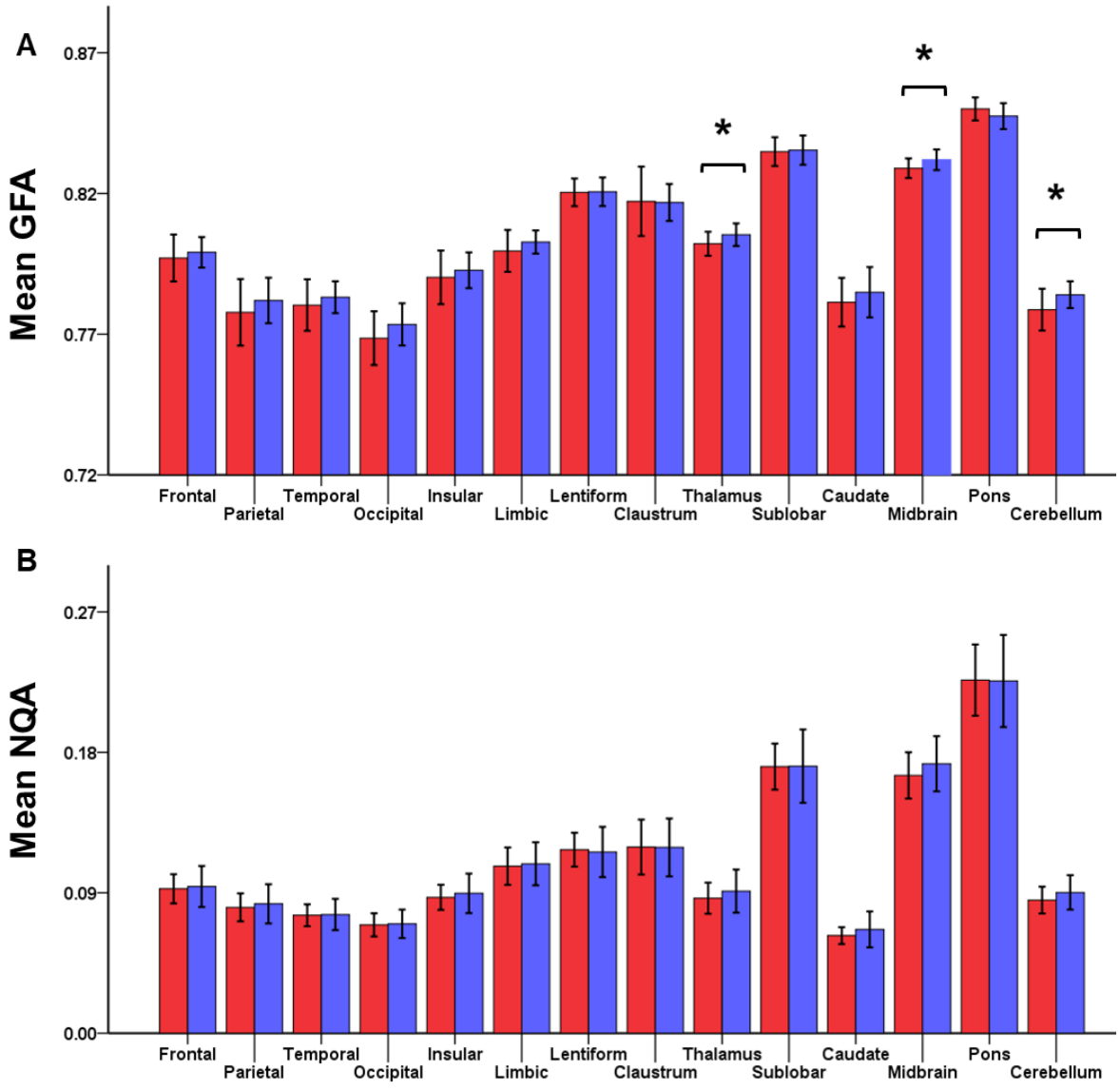

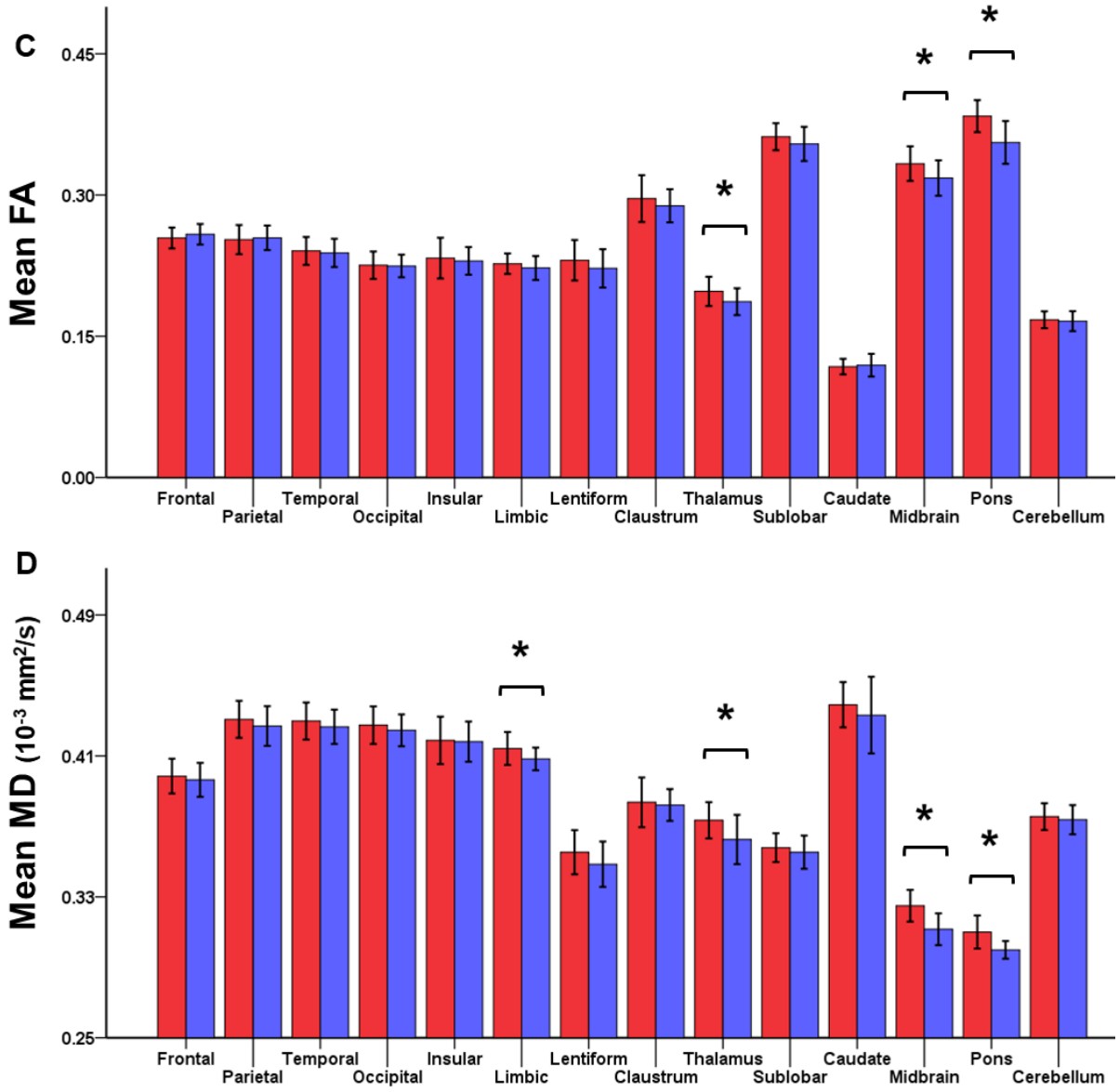

Figure 3. Bar graphs showing the mean (A) generalized fractional anisotropy (GFA), (B) normalized quantitative anisotropy (NQA), (C) fractional anisotropy (FA), and (D) mean diffusivity (MD) in women (red) and men (blue). The whiskers indicate standard deviation (SD). * and brackets indicate statistical significance (two sample t-tests, uncorrected $P < 0.05$) (Abbreviations: Frontal = frontal lobe, Parietal = parietal lobe, Temporal = temporal lobe, Occipital = occipital lobe, Insular = insular lobe, Limbic = limbic lobe, Caudate = caudate nucleus, Lentiform = lentiform nucleus, Sublobar = sublobar white matter).

3.3. Correlation of DSI indices with age

Table 2 summarizes the results of correlation of diffusion indices with age. Significant GFA decrease with age was observed in the sublobar white matter ($r = -0.525$, corrected $P = 0.017$). On the other hand, significant age-related GFA increase was observed in the lentiform nucleus ($r = 0.540$, corrected $P = 0.011$). As for NQA, there was a significant decrease with age in the frontal ($r = -0.543$, corrected $P = 0.011$), temporal ($r = -0.534$, corrected $P = 0.014$), and occipital ($r = -0.521$, corrected $P = 0.018$) lobes, sublobar white matter ($r = -0.643$, corrected $P < 0.001$), and caudate nucleus ($r = -0.563$, corrected $P = 0.006$). FA decreased significantly in the frontal lobe ($r = -0.502$, corrected $P = 0.029$) and sublobar white matter ($r = -0.515$, corrected $P = 0.022$) and increased significantly in the lentiform nucleus ($r = 0.484$, corrected $P = 0.045$), with age. For MD, significant decrease with age was observed only in the lentiform nucleus ($r = -0.575$, corrected $P = 0.004$).

Table 2. Relationship of the mean GFA, NQA, FA, and MD with age.

Anatomical location	GFA	NQA	FA	MD
Frontal lobe	-0.260	**-0.543**	**-0.502**	-0.076
Parietal lobe	-0.131	-0.471	-0.239	-0.082
Temporal lobe	-0.133	**-0.534**	-0.350	-0.086
Occipital lobe	-0.306	**-0.521**	-0.397	0.109
Insula	0.000	-0.319	-0.148	-0.095
Limbic lobe	-0.104	-0.417	-0.252	-0.038
Lentiform nucleus	**0.540**	-0.083	**0.484**	**-0.575**
Claustrum	-0.166	-0.421	-0.078	-0.130
Thalamus	-0.238	-0.462	-0.346	0.317
Sublobar white matter	**-0.525**	**-0.643**	**-0.515**	0.327
Caudate nucleus	-0.238	**-0.563**	-0.253	0.133
Midbrain	0.093	-0.258	0.160	-0.131
Pons	-0.148	-0.352	-0.083	-0.148
Cerebellum	-0.025	-0.244	0.007	-0.115

Note: numbers in bold indicate statistical significance (corrected $P < 0.05$). GFA = generalized fractional anisotropy, NQA = normalized quantitative anisotropy, FA = fractional anisotropy, MD = mean diffusivity

4. Discussion

Variation of GFA, NQA, FA, and MD with anatomical location, gender, and age was observed in the present study. This indicates that interpretation of DSI indices will require normative reference values for particular anatomical location, gender, and age. The results of this study may serve as reference values.

Regional FA and MD variation has been reported in several DTI studies, in particular the difference between white and gray matter. Several findings in this study agree with those of several previous DTI studies. For example, lower FA was observed in the caudate nucleus and cerebellum than the frontal, parietal, temporal lobes, thalamus, corpus callosum, and cingulum. The corpus callosum had the highest FA (Das et al., 2017; Lätt et al., 2013; Panesar et al., 2017). The lentiform nucleus had lower MD than the thalamus (Lee et al., 2009). These differences have been considered as due to regional variation in fiber density or myelination. Supportive of this, studies have shown positive correlations among FA, axon density, and myelin content (Friedrich et al., 2020). The present study adds some new findings, such as GFA and NQA differences among the major cerebral lobes. It was observed that GFA and NQA were higher in the frontal lobe and lower in the occipital lobe, than in the parietal and temporal lobes. These observations are in agreement with a postmortem study which observed a larger and a lower number of glial cells including oligodendrocytes in the frontal lobe and the occipital lobe, respectively (Karlsen and Pakkenberg, 2011). Oligodendrocytes are the glial cells that produce myelin (Compston et al., 1997).

The present study also revealed gender variation in GFA, FA, and MD in several anatomical locations. Women had higher MD in the limbic lobe, which agrees with the observation of a previous study (Huster et al., 2009). Higher GFA in the cerebellum in men and higher FA in pons in women were also observed, which may imply differential brain functioning between the two gender groups. A previous neuropsychological study has reported that men have a higher performance in spatial navigation and women have a higher performance in finger dexterity (Kimura, 1996). Since the cerebellum and pons contribute to spatial navigation and visual control of movement respectively, it is possible that structural variation

may underlie differential brain functioning between the two gender groups (Maraganore et al., 1992; Rochefort, Lefort, and Rondi-Reig, 2013). A few contradictory observations among GFA, FA, and MD were also observed in this study. For example, women had higher FA and MD, but lower GFA in the midbrain, than men (Menzler et al., 2011; Takao, Hayashi, and Ohtomo, 2014). This may be because DTI cannot distinguish crossing fibers and neurites aligned in several orientations.

Apart from the variations of DSI indices with anatomical location and gender, the present study also observed an age-dependent decrease in GFA, NQA, and FA in the majority of anatomical locations. These findings are in agreement with several previous DTI studies, which report an FA decrease in the superior frontal and temporal gyri, middle occipital gyrus, postcentral gyrus, corpus callosum, corticospinal tract, and superior fronto-occipital fasciculus (Bhagat and Beaulieu, 2004; Liu et al., 2018). Age-related decreases in GFA, NQA, and FA are thought to reflect neuronal and myelin loss. A previous histologic study on human brains has reported an increased percentage of nonmyelinated nerve fibers with age in the corpus callosum (Meier-Ruge, et al., 1992). Animal experiments on rhesus monkeys have also observed a correlation in the cellular aging of white matter with a decrease in the number of myelinated nerve fibers and an increase in the number of axons (Bowley et al., 2010; Sandell and Peters, 2003). Myelin water fraction imaging has also shown an age-related decrease in myelin in the corpus callosum, and the frontal, parietal, and occipital white matter of healthy volunteers aged 18-79 years (Faizy et al., 2020). Interestingly, age-related GFA and FA increase was only observed in the lentiform nucleus. FA increase with age has been reported in a previous DTI study (Bhagat and Beaulieu, 2004). Mechanisms underlying age-related GFA and FA increase are not known, which demands further exploration. In addition, significant correlations of NQA with age were observed in the frontal and temporal lobes, but not the parietal lobe. According to a previous report, a linear decrease in brain weight along with a decrease in cortical thickness is observed from 24 through 100 years of age, and this decrease is more conspicuous in the frontal and temporal lobes than in parietal lobes (Terry, DeTeresa, and Hansen, 1987).

Several limitations need to be addressed. First, the sample size of this study is small. Three

of 39 participants had to be excluded due to motion artifacts probably associated with a long acquisition time. Further reduction in TA may alleviate such artifacts. Second, this study included only adults aged from 20 to 65 years old. The observations may not represent the elderly (i.e. age over 65 years) (Orimo, 2006). Third, this study observed variations in DSI indices with anatomical location, gender, and age. Although it is speculated that these variations are related to changes or differences in axonal and myelin density, this study cannot determine the exact underlying mechanisms. Combined evaluation with other MRI imaging techniques that quantify axon and myelin may be helpful.

5. Conclusions

This study evaluated the variation in GFA and NQA, along with FA and MD, with anatomical location, gender, and age. The results suggest location, gender, and age dependency of these indices. Thus, their interpretation in normal or pathological state would require normative reference values. The results of this study may serve as reference values.

Chapter 2.

Microstructural attributes of hemispheric lateralization: a combined evaluation of diffusion spectrum imaging and MR spectroscopic imaging

1. Introduction

The human brain exhibits hemispheric lateralization, that is one cerebral hemisphere being dominant than the other. A well-known example of hemispheric lateralization is that of the language area. In the majority of the population, Broca's area which is the primary language area is located in the left frontal operculum (Turkeltaub and Coslett, 2010). Other examples of hemispheric lateralization are the lateralization in the depth of the central sulcus and the size of the hippocampus. A leftward asymmetry exists in the depth of the central sulcus in right-handers at dorsal levels (Amunts et al., 1996). The left hippocampus is reported as smaller than the right in male (Jack et al., 1989).

The knowledge about hemispheric lateralization is important to prevent important functional areas from accidentally damaging during surgery as well as to avoid misinterpretation of normal laterality as pathological or vice versa. To explain further, injury to the right frontal operculum may not lead to motor aphasia, whereas that to the left may injure the Broca's area to cause aphasia (Alexander, Naeser, and Palumbo, 1990; Nitta et al., 2012). The normal right-greater-than-left asymmetry of the hippocampus may mimic left mesial temporal sclerosis, and the left mesial temporal sclerosis may be falsely interpreted as the normal right-greater-than-left asymmetry (Jack et al., 1989; Van Paesschen et al., 1997).

It has been believed that hemispheric lateralization results from differences in neural architecture at the molecular or cellular level between the two hemispheres. Although there have been several studies that document differences between the two hemispheres through histological and electron microscopic findings (Cullen et al., 2006; Uylings et al., 2006), thorough investigations about lateralization in neural architecture across the whole hemisphere are scarce. In this prospective study, hemispheric lateralization in the neural architecture was

detected by using DSI and DTI indices because these indices are known to represent cellular arrangement and density. The extent of laterality in these indices was determined, and similarity in the pattern of lateralization with that of neurometabolite concentrations was evaluated. Neurometabolites are the essential components of neurons and glia, and their concentrations also reflect the integrity of the neural architecture.

2. Materials and methods

2.1. Participants

This prospective study was approved by the institutional review board of Hokkaido University. Written informed consent was obtained from all participants. Volunteers were recruited over a recruitment period of 21 months (2016/07 ~ 2018/03). The inclusion criteria were aged from 20 to 65 years old and confirmed right-handedness, as evaluated by the Edinburgh Handedness Inventory (Oldfield, 1971). The exclusion criteria included absolute contraindications for MRI, history of diseases that might affect the integrity of the central nervous system, gross abnormalities on conventional MR images, and visible motion artifacts on diffusion images. Of 30 volunteers who consented to the study, one volunteer was excluded because of brain motion artifacts. This resulted in a total of 29 right-handed participants (14 women and 15 men; age range = 22-60 years, mean age ± SD = 33.97 ± 11.10 years).

2.2. MRI

MRI was performed using a 3T scanner (MAGNETOM Prisma, Siemens Healthcare, Erlangen, Germany) and a 64-channel head/neck coil.

The acquisition parameters of DSI and several other sequences used in this study (i.e., MPRAGE, FLAIR, and PDWI) are as detailed in Chapter 1. To measure neurometabolites, whole-brain magnetic resonance spectroscopic imaging (WB-MRSI) was acquired using a prototype echo-planar spectroscopic imaging sequence with water suppression and lipid inversion nulling (TR/TE/TI = 1710 ms/17 ms/198 ms, flip angle = 73°, voxel size = 5.6 × 5.6 × 10 mm^3, TA = 16:49 min). The WB-MRSI acquisition also included an interleaved water

reference of the same dimensions as the metabolites WB-MRSI, which was acquired using a gradient-echo acquisition without water suppression (flip angle = 10°, TE = 3.8 ms). The data were acquired for the normalization of neurometabolite concentrations (Ding et al., 2015). A radiologist with 19-year experience in neuroimaging reviewed the images to exclude the abnormalities and artifacts.

2.3. Data processing

The processing steps are summarized in Figure 1.

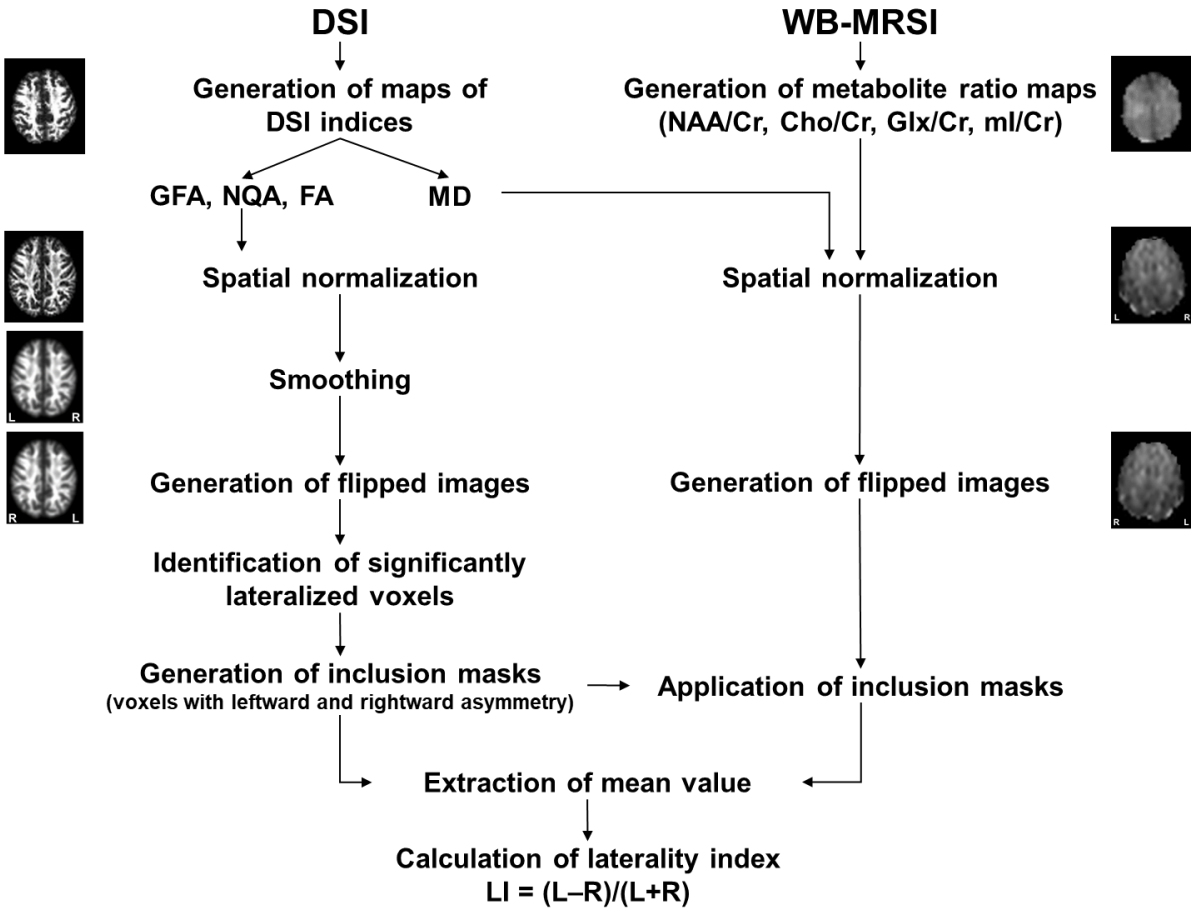

Figure 1. Scheme summarizing the processing steps (Abbreviations: DSI = diffusion spectrum imaging, GFA = generalized fractional anisotropy, NQA = normalized quantitative anisotropy, FA = fractional anisotropy, MD = mean diffusivity, LI = laterality index, WB-MRSI = whole-brain magnetic resonance spectroscopic imaging, NAA = N-acetyl aspartate, Cho = choline, Cr = creatine, Glx = glutamate and glutamine compounds, mI = myoinositol)

2.3.1. Pre-processing of DSI data

The DSI and DTI indices, that is GFA, NQA, FA, and MD maps, were reconstructed and were spatially normalized to remove individual differences in anatomy. Generation of a brain parenchyma mask followed. The details about all these processes are as detailed in Chapter 1. The spatially normalized GFA, NQA, and FA maps were then smoothed with a Gaussian kernel of 5 mm full width at half maximum (FWHM) (SPM12) to increase the signal-to-noise ratio (SNR). Next, flipped images of spatially normalized GFA, NQA, FA, and MD maps, and smoothed GFA, NQA, and FA maps were generated (MRICron version 1.0, Chris Rorden's Neuropsychology Lab, University of South Carolina, Columbia, USA) (Rorden, Karnath, and Bonilha, 2007). Finally, a brain parenchyma mask was applied to the non-flipped and flipped GFA, NQA, FA, and MD maps.

2.3.2. Pre-processing of WB-MRSI data

The major neurometabolite maps, including N-acetyl aspartate (NAA), choline (Cho), creatine (Cr), glutamate and glutamine compounds (Glx), and myoinositol (mI), were reconstructed from the WB-MRSI raw data, using the default parameters of Metabolic Imaging and Data Analysis System (MIDAS) software version 2.35 (University of Miami, Miami, Florida, US) which runs on IDL version 8.4.1(Exelis Visual Information Solutions, Boulder, Colorado, US) (Maudsley et al., 2009). The processing steps included B_0 and frequency shift correction, lipid K-space extrapolation, and parametric spectral fitting. As a measure of spectral quality control (i.e., to maintain SNR), spectra with a linewidth (i.e., FWHM of the metabolic peak's height) greater than 13 Hz were excluded (Birch et al., 2017). The neurometabolite ratio maps (NAA/Cr, Cho/Cr, Glx/Cr, and mI/Cr) were then reconstructed from the corresponding neurometabolite maps (SPM12), which were used in further data analyses. Spatial normalization was applied to reconstructed neurometabolite ratio maps (SPM12). Voxels other than the brain tissues in the normalized neurometabolite ratio maps were removed by applying a brain parenchyma mask used in the DSI processing steps and discarding the voxels with signal intensity beyond 2.5 and 97.5% of the total signal intensity distribution in each map (ImageJ),

followed by the generation of flipped images for each non-flipped normalized metabolite ratio maps.

2.3.3. Identification of voxels with hemispheric lateralization

Pre-processed non-flipped and flipped GFA, NQA, and FA maps were compared voxel-by-voxel for any hemispheric lateralization, using paired t-tests (familywise error corrected $P < 0.05$, cluster size ≥ 50 voxels) (SPM12). Of voxels with significant hemispheric lateralization, voxels with larger values in the left hemisphere were regarded as leftward asymmetry, and those with larger values in the right hemisphere as rightward asymmetry. Inclusion masks covering these voxels were then generated (SPM12). These inclusion masks were applied onto the spatially normalized non-flipped and flipped GFA, NQA, and FA maps, and their mean values were extracted (MRICron). From the extracted mean values, laterality index (LI) was calculated using the formula $LI = (L–R)/(L+R)$, where L and R indicate the mean value of voxels with significant leftward and rightward asymmetry on the GFA, NQA, or FA map, respectively. LI ranged from -1 to 1, where voxels with leftward asymmetry were assigned values larger than 0 and those with rightward asymmetry values smaller than 0.

To further explore if hemispheric lateralization of GFA, NQA, and FA had a relationship with lateralization of MD and neurometabolite ratios, the aforementioned inclusion masks were applied onto the non-flipped and flipped MD and neurometabolite ratio maps. The mean values under each mask were then extracted, and LI was calculated (MRICron). As above, further analyses were limited to voxels containing at least 30% of brain tissue fraction (MRICron). Lateralization was tested using one sample t-tests (uncorrected $P < 0.05$). Statistical analyses were carried out using SPSS software version 22.

3. Results

3.1. Identification of voxels with hemispheric lateralization in GFA, NQA, and FA maps

Voxels with significant leftward and rightward asymmetry on GFA, NQA, and FA maps are shown in Figure 2 and Table 1.

Leftward GFA asymmetry was observed in the posterior cingulate cortex {$T_{(28)}$ = 12.52, 610 voxels, MNI coordinates: X = -20, Y = -54, Z = 14; $T_{(28)}$ = 9.87, 104 voxels, X = -18, Y = -26, Z = 42}, the thalamus {$T_{(28)}$ = 12.89, 404 voxels, MNI coordinates: X = -18, Y = -16, Z = 0}, and hippocampus {$T_{(28)}$ = 10.02, 54 voxels, MNI coordinates: X = -30, Y = -10, Z = -14}. Leftward NQA asymmetry was observed in the thalamus {$T_{(28)}$ = 12.97, 751 voxels, MNI coordinates: X = -26, Y = -24, Z = 12}, posterior cingulate cortex {$T_{(28)}$ = 12.91, 741 voxels, MNI coordinates: X = -8, Y = -44, Z = 20; $T_{(28)}$ = 10.38, 153 voxels, X = -16, Y = -26, Z = 42}, midbrain {$T_{(28)}$ = 9.63, 87 voxels, MNI coordinates: X = -4, Y = -32, Z = -22}, Rolandic operculum {$T_{(28)}$ = 9.32, 85 voxels, MNI coordinates: X = -46, Y = -10, Z = 20}, medial frontal gyrus {$T_{(28)}$ = 10.81, 61 voxels, MNI coordinates: X = -14, Y = 38, Z = 20}, and lentiform nucleus {$T_{(28)}$ = 9.51, 60 voxels, MNI coordinates: X = -26, Y = 8, Z = 4}. Leftward FA asymmetry was observed in the thalamus {$T_{(28)}$ = 15.65, 1182 voxels, MNI coordinates: X = -18, Y = -18, Z = 0}, posterior cingulate cortex {$T_{(28)}$ = 13.38, 820 voxels, MNI coordinates: X = -20, Y = -54, Z = 16; $T_{(28)}$ = 10.08, 58 voxels, MNI coordinates: X = -14, Y = -18, Z = 42}, pons {$T_{(28)}$ = 12.22, 66 voxels, MNI coordinates: X = -4, Y = -36, Z = -30}, and Rolandic operculum {$T_{(28)}$ = 9.37, 55 voxels, MNI coordinates: X = -44, Y = -10, Z = 20}.

On the other hand, rightward GFA asymmetry was observed in the superior temporal gyrus {$T_{(28)}$ = 18.91, 904 voxels, MNI coordinates: X = 34, Y = 4, Z = -14}, frontal white matter {$T_{(28)}$ = 9.26, 91 voxels, MNI coordinates: X = 38, Y = -16, Z = 34}, putamen {$T_{(28)}$ = 12.93, 61 voxels, MNI coordinates: X = 20, Y = 2, Z = -4}, and superior frontal gyrus {$T_{(28)}$ = 11.90, 52 voxels, MNI coordinates: X = 20, Y = 22, Z = 38}. Rightward NQA asymmetry was observed in the sublobar white matter {$T_{(28)}$ = 14.56, 730 voxels, MNI coordinates: X = 36, Y = -22, Z = 0}, superior temporal gyrus {$T_{(28)}$ = 18.68, 255 voxels, MNI coordinates: X = 34, Y = 4, Z = -14}, frontal white matter {$T_{(28)}$ = 11.56, 101 voxels, MNI coordinates: X = 40, Y = -16, Z = 34}, and superior frontal gyrus {$T_{(28)}$ = 9.38, 59 voxels, MNI coordinates: X = 22, Y = 16, Z = 40}. Rightward FA asymmetry was observed in the superior temporal gyrus {$T_{(28)}$ = 14.06, 1206 voxels, MNI coordinates: X = 52, Y = -22, Z = 6; $T_{(28)}$ = 14.96, 284 voxels, MNI coordinates: X = 34, Y = 4, Z = -22}, parahippocampal gyrus {$T_{(28)}$ = 12.15, 92 voxels, MNI

coordinates: X = 26, Y = -22, Z = -18}, frontal white matter {$T_{(28)}$ = 11.43, 61 voxels, MNI coordinates: X = 38, Y = -16, Z = 34}, and cerebellum {$T_{(28)}$ = 8.89, 52 voxels, MNI coordinates: X = 22, Y = -34, Z = -32}.

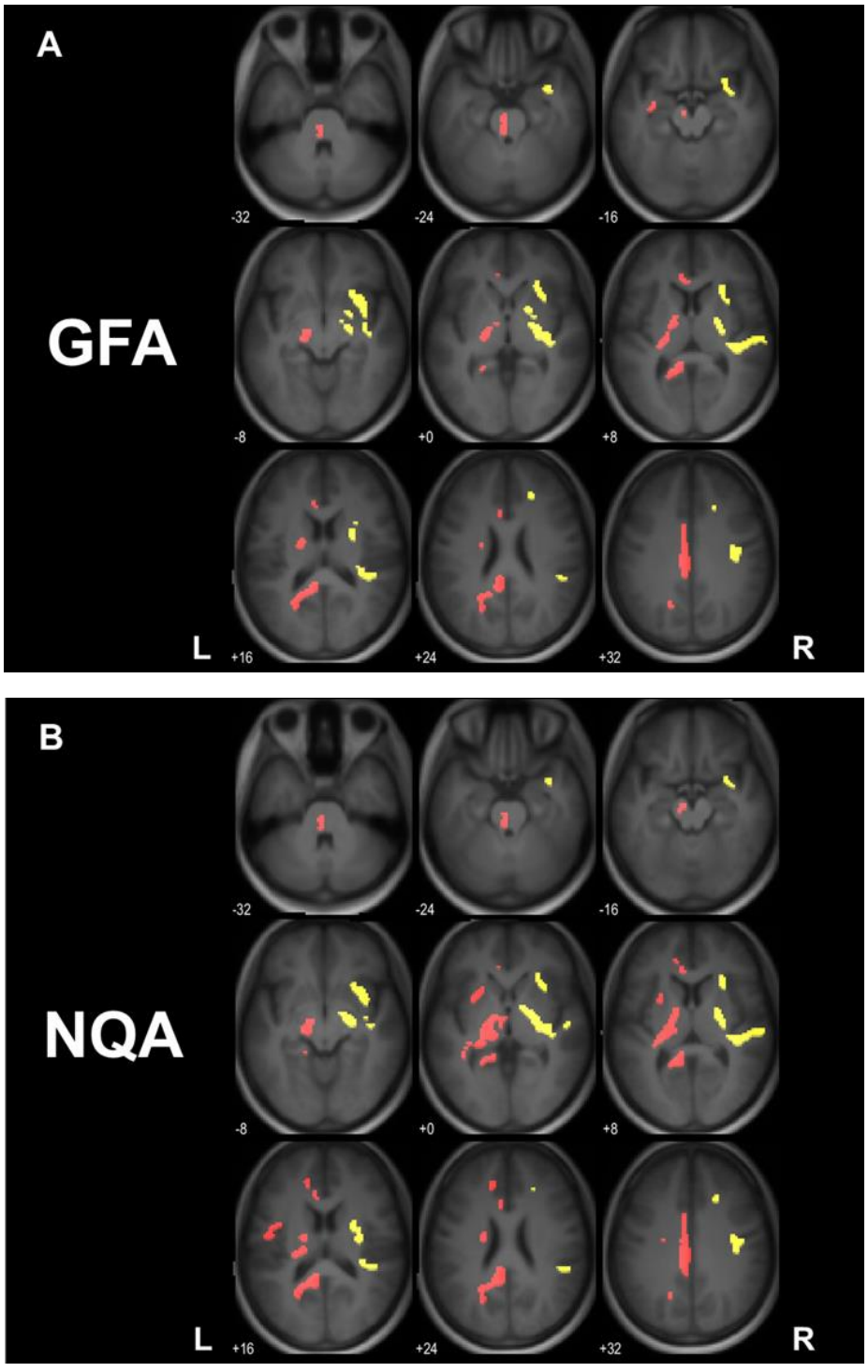

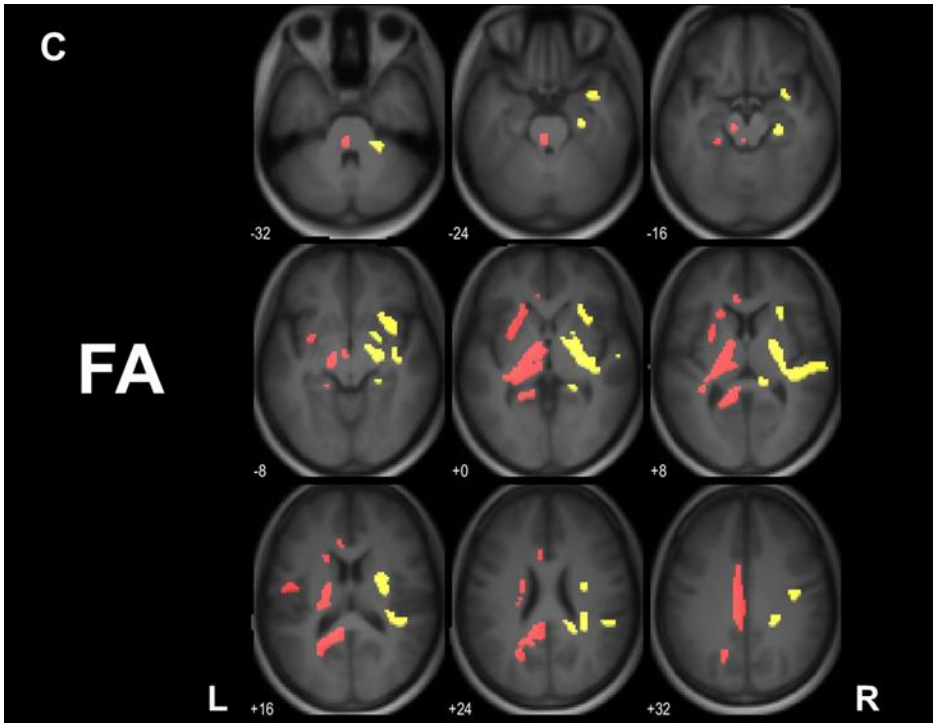

Figure 2. The clusters showing voxels with significant leftward (red) and rightward (yellow) asymmetry on the (A) generalized fractional anisotropy (GFA), (B) normalized quantitative anisotropy (NQA), and (C) fractional anisotropy (FA) maps (familywise error corrected $P < 0.05$). The clusters are shown as overlay on a 3-dimensional (3D) magnetization prepared rapid acquisition gradient-echo (MPRAGE) template. L and R indicate left and right, respectively.

Table 1. Clusters with significant leftward and rightward hemispheric asymmetry in GFA, NQA, and FA maps.

Index	Asymmetry	Anatomical location	MNI coordinates			Cluster size	T value
			X	Y	Z		
GFA	Leftward	Posterior cingulate cortex	-20	-54	14	610	12.52
		Thalamus	-18	-16	0	404	12.89
		Posterior cingulate cortex	-18	-26	42	104	9.87
		Hippocampus	-30	-10	-14	54	10.02
	Rightward	Superior temporal gyrus	34	4	-14	904	18.91
		Frontal white matter	38	-16	34	91	9.26
		Putamen	20	2	-4	61	12.93
		Superior frontal gyrus	20	22	38	52	11.90
NQA	Leftward	Thalamus	-26	-24	12	751	12.97
		Posterior cingulate cortex	-8	-44	20	741	12.91
		Posterior cingulate cortex	-16	-26	42	153	10.38
		Midbrain	-4	-32	-22	87	9.63
		Rolandic operculum	-46	-10	20	85	9.32
		Medial frontal gyrus	-14	38	20	61	10.81
		Lentiform nucleus	-26	8	4	60	9.51
	Rightward	Sublobar white matter	36	-22	0	730	14.56
		Superior temporal gyrus	34	4	-14	255	18.68
		Frontal white matter	40	-16	34	101	11.56
		Superior frontal gyrus	22	16	40	59	9.38
FA	Leftward	Thalamus	-18	-18	0	1182	15.65
		Posterior cingulate cortex	-20	-54	16	820	13.38
		Pons	-4	-36	-30	66	12.22
		Posterior cingulate cortex	-14	-18	42	58	10.08
		Rolandic operculum	-44	-10	20	55	9.37
	Rightward	Superior temporal gyrus	52	-22	6	1206	14.06
		Superior temporal gyrus	34	4	-22	284	14.96
		Parahippocampal gyrus	26	-22	-18	92	12.15
		Frontal white matter	38	-16	34	61	11.43
		Cerebellum	22	-34	-32	52	8.89

Note: GFA = generalized fractional anisotropy, NQA = normalized quantitative anisotropy, FA = fractional anisotropy, MNI = Montreal Neurological Institute

3.2. Relationship of lateralization of GFA, NQA, and FA with MD and neurometabolite ratios

The LI of GFA, NQA, FA, MD, and neurometabolite ratios are shown in Figure 3. Voxels with leftward lateralization in GFA, NQA, and FA exhibited rightward MD lateralization ($P < 0.001$), leftward NAA/Cr lateralization ($P < 0.001$), and no significant lateralization in Cho/Cr, Glx/Cr, and mI/Cr. Voxels with rightward lateralization in GFA, NQA, and FA exhibited leftward lateralization in MD ($P < 0.001$) and Glx/Cr ($P < 0.001$) and rightward Cho/Cr lateralization ($P < 0.001$). Only voxels with rightward NQA lateralization exhibited rightward NAA/Cr lateralization ($P = 0.014$). There was no mI/Cr lateralization in voxels with rightward lateralization in GFA, NQA, and FA.

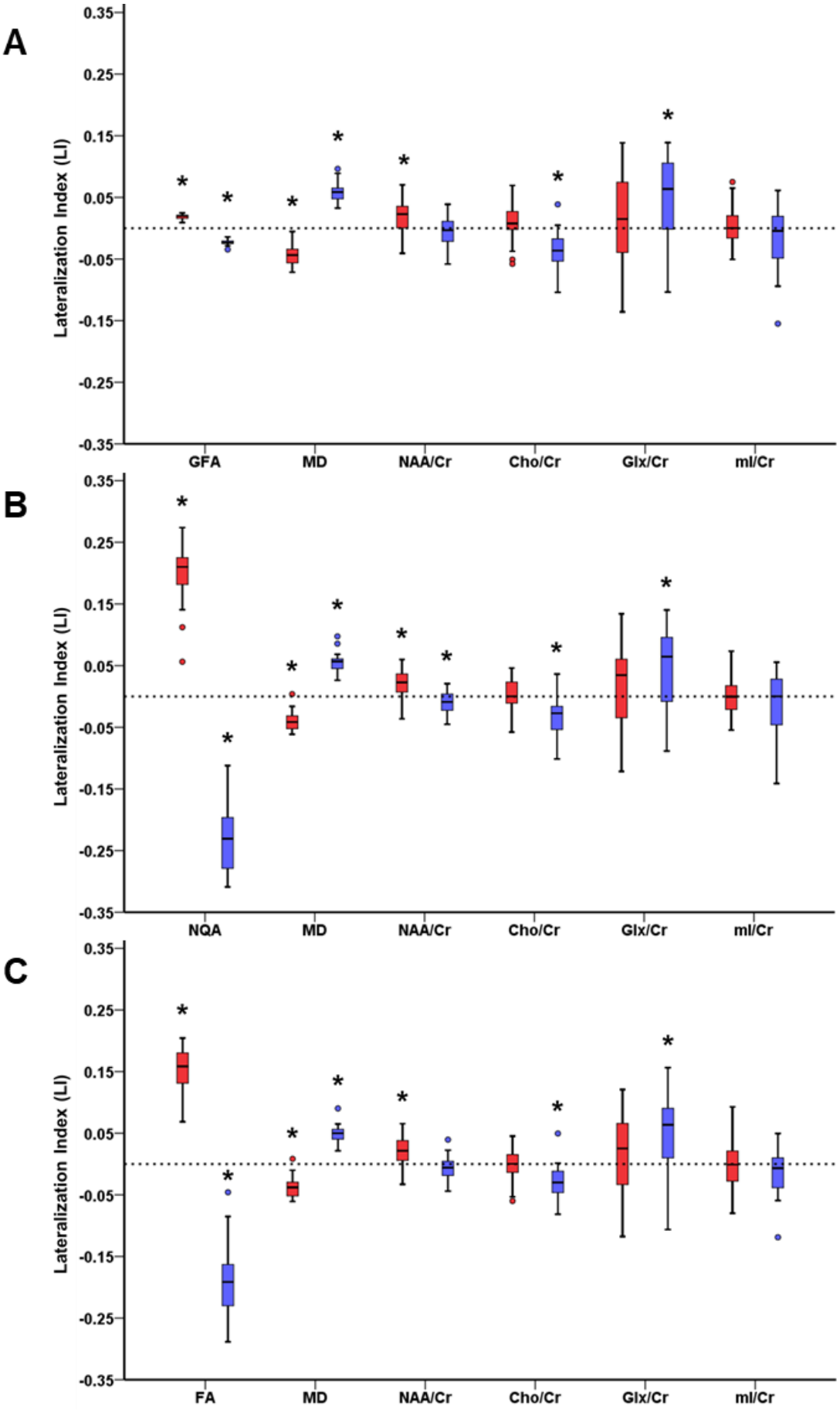
A
B
C
Lateralization Index (LI)
0.35
0.25
0.15
0.05
-0.05
-0.15
-0.25
-0.35
GFA
MD
NAA/Cr
Cho/Cr
Glx/Cr
mI/Cr
NQA
FA

Figure 3. Box and whisker plots showing the median, interquartile range, minimum, and maximum for the laterality index (LI) of mean diffusivity (MD) and neurometabolite ratio maps calculated in voxels with leftward (red) and rightward asymmetry (blue) of the (A) generalized fractional anisotropy (GFA), (B) normalized quantitative anisotropy (NQA), and (C) fractional anisotropy (FA) maps. Whiskers indicate standard deviation (SD). The dotted line demarcates the LI at 0. * indicates statistical significance (one sample t-tests, uncorrected $P < 0.05$) {Abbreviations: N-acetyl aspartate (NAA), choline (Cho), creatine (Cr), glutamate and glutamine compounds (Glx), and myoinositol (mI)}.

4. Discussion

The present study evaluated hemispheric lateralization in the neural architecture by using DSI and DTI indices. There were many voxels with GFA, NQA, and FA lateralization. A similar pattern of lateralization was observed between these indices and NAA/Cr, whereas a reverse pattern was observed with MD, Glx/Cr, and Cho/Cr.

GFA, NQA, and FA exhibited a similar pattern of lateralization with NAA/Cr. NAA is synthesized in the mitochondria and located predominantly in neurons. It is often regarded as the marker of neuron density (Bjartmar et al., 2002). A higher NAA often indicates a larger number of healthy neurons and vice versa. For example, NAA increases with development and declines with age; infants and the elderly have a lower local NAA than middle-aged adults. Cr is known to be the marker of energy metabolism. The Cr levels tend to be stable across normal and various pathological states so that Cr is commonly used as the denominator to normalize neurometabolite concentrations. Since GFA, NQA, and FA are reflective of neuronal integrity in terms of cell number or alignment, it is plausible that these indices exhibit a similar pattern of hemispheric lateralization with NAA/Cr. The observation of the reverse pattern of MD lateralization can also be explained by the difference in cell density between the two hemispheres, as MD is known to be negatively associated with cell density. Cho is often considered a marker of myelin and cell membrane. It mainly contains phosphorylcholine and glycerol-phosphorylcholine, the former being the major Cho metabolite. It is likely that regions

with dense neuron populations have denser myelin, so as to result in a difference in Cho concentration between the two hemispheres. From the fact that phosphorylcholine is not detectable by MRI when embedded in myelin, cell membranes, and other complex brain lipids (Pouwels and Frahm, 1998) and the observation of a similar pattern of Cho/Cr lateralization with that of GFA, NQA, and FA, it is thought that a difference in free Cho content, not that embedded in myelin, produced the difference. The cause of the reverse pattern of lateralization of Glx/Cr is less understood. The main component of Glx is glutamate, which is an excitatory neurotransmitter mainly located in the nerve terminals of the synapse (Cullen et al., 2006; Uylings et al., 2006). It is thus expected to find a higher Glx/Cr in regions with densely populated neurons. Extended studies are necessary to confirm the observed relationship. mI is a glial cell marker. Lack of hemispheric mI/Cr may imply that the number of glial cells in both left and right hemispheres is relatively stable.

This study showed many voxels with hemispheric lateralization of GFA, NQA, and FA. The observation of leftward FA lateralization in the thalamus is in agreement with that of a previous DTI report (Takao et al., 2011). Similarly, leftward lateralization of GFA and the tract volume (Chiu et al., 2011; Wakana et al., 2007) and rightward lateralization of MD (Das et al., 2017) in the cingulate gyrus, and leftward FA asymmetry and the tract volume (Brander et al., 2010; Thiebaut de Schotten et al., 2011b) and rightward MD asymmetry (Brander et al., 2010) in the motor pathway, greater FA in the putamen and superior longitudinal fasciculus (Das et al., 2017; Park et al., 2004) have been reported. Collectively considering hemispheric lateralization of GFA, NQA, and FA and that of neurometabolite concentrations, it is thought that regions with higher GFA, NQA, FA, NAA/Cr, and lower MD are composed of tightly packed highly aligned neurons (Sun and Walsh, 2006). The reverse will also be true for regions with lower GFA, NQA, FA, NAA/Cr, and higher MD. The left thalamus, left cingulate gyrus, and some areas of the motor pathway such as the left half of the midbrain and pons may have more tightly packed highly aligned neurons than the right, and vice versa for uncinate fasciculus, putamen, frontal eye fields in the superior frontal gyrus, and superior longitudinal fasciculus. Supportive of our speculation, a post mortem study has shown larger fiber size and number in

the right uncinate fasciculus (Highley et al., 2002).

Handedness may be related to at least some observations. For example, leftward lateralization in the given DSI indices of the motor pathway and Rolandic operculum may be because the left cerebral hemisphere is the dominant hemisphere in right-handers (Turkeltaub and Coslett, 2010). Lateralization in tissue architecture may have implications in brain functioning.

There are a few potential limitations. First, only right-handers were included in this study. The results derived from left-handers may be different from right-handers. Second, only neurometabolite ratios, instead of absolute neurometabolite concentrations, were evaluated in this study because neurometabolite ratios are more commonly used in real clinical situations than neurometabolite concentrations. However, this may result in the difficulty in interpretation of alteration for neurometabolites because it is not easily known which neurometabolite (i.e., the numerator or denominator) is responsible for the observation.

5. Conclusion

There is widespread lateralization of the diffusion indices across cerebral hemispheres. The pattern of lateralization of these indices follows that of some neurometabolites. Combined evaluation with neurometabolites has provided more complete information about the composition of neural architecture.

Chapter 3.

Tissue microstructural changes following four-week cognitive training: observations of double diffusion encoding MRI

1. Introduction

Improved cognitive performance after a certain period of cognitive training has been reported in both normal and cognitively impaired individuals (Ghio et al., 2018; Verhelst et al., 2019). Regarding training duration, improved cognitive performance has been reported with three weeks or longer training duration (Lampit et al., 2015). It is important to study how cognitive training alters brain structure and function. MRI has been widely used to study the cognitive training-derived neuroplastic changes in the brain. According to previous reports, a 3-week cognitive training involving action-related verbs resulted in increased gray matter volume in the left dorsal precentral gyrus and the right cerebellar hemisphere (Ghio et al., 2018). Another 3-week cognitive training involving exercises of memory, attention, response speed, executive functions, and language improved functional connectivity between the right hippocampus and the left superior temporal gyrus (Lampit et al., 2015). This evidence suggests that MRI can provide information about neural pathways associated with improved training-derived cognitive performance.

In addition to the above, cognitive training-derived neuroplastic changes have also been reported in several DTI studies. For example, increased FA in the right precentral gyrus and decreased MD in the left superior longitudinal fasciculus associated with improved information processing speed and verbal working memory were observed in the patients with traumatic brain injury after an 8-week cognitive training (Verhelst et al., 2019). In another study, increased FA in the left superior longitudinal fasciculus that was associated with improved performance in innovative decision-making were observed in normal adults after a 4-week cognitive training of working memory, attention, and inhibition control (Crespi et al., 2018). Cognitive training-derived neuroplastic changes in DTI indices have also been reported to

associate with changes in neuronal or axonal architecture in animal experiments. A previous histological study on rats has reported increased FA in the corpus callosum and decreased MD in the hippocampus brains was associated with increased, volume and perimeter of synapses and astrocytes, and organization and packing of axons or myelin after a learning and memory training (Blumenfeld-Katzir et al., 2011). These findings support the suitability of DTI to characterize the cognitive training-derived neuroplastic changes noninvasively. However, considering the limitation of DTI in evaluating orientation dispersion, DDE MRI may provide more accurate information about the cognitive training-derived neuroplastic changes. Nevertheless, to our knowledge, there have been no reports that evaluate these changes by using DDE MRI.

This study hypothesized that DDE MRI outperforms DTI in identifying cognitive training-derived neuroplastic changes. The purpose is to compare the performance of μFA, FA, and MD in illustrating cognitive training-derived neuroplastic changes after 4-week attention and working memory training in healthy young adults.

2. Materials and methods

2.1. Participants

This prospective study was approved by the institutional review board of Hokkaido University. Written informed consent was obtained from all participants. Volunteers were recruited over a recruitment period of 16 months (2018/07 ~ 2019/10). The inclusion criterion was age over 20 years. The exclusion criteria included absolute contraindications for MRI, a history of diseases that might affect the integrity of the central nervous system, and previous experience with cognitive training (Rebok et al., 2014). To evaluate cognitive training-derived neuroplastic changes and the relationship between these changes and the training performance, participants were divided into training and control groups. The sample size needed for this study was estimated using G power 3.0 (Faul et al., 2009), based on a prospective internal pilot study using ROI-based analysis {Eight participants were randomly assigned to the training and control groups. μFA measurable at the frontal lobes was used to estimate sample size, as the

frontal lobe is associated with attention and working memory function (Owen et al., 1998; Rossi et al., 2009)}. To achieve the statistical power of 0.95, six participants would be necessary for each group for observation of cognitive training-derived DDE MRI changes, at effect size f = 0.587. In addition, 16 participants would be necessary for the training group for observation of the correlation between the training-derived DDE MRI indices and cognitive improvement, at effect size |r| = 0.660. Considering drop-out, 23 volunteers were recruited for the training group and eight volunteers for the control group. Two participants from the training group were excluded due to incomplete cognitive training. This resulted in a total of 21 participants {9 female and 12 male; age range = 22-40 years; mean age ± SD = 27.7 ± 6.0 years; mean years of education ± SD = 15.7 ± 0.5 years} were included in the training group, and 8 age, sex, and education level-matched participants (4 female and 4 male; age range = 22-52 years; mean age ± SD = 31.5 ± 9.5 years; mean years of education ± SD = 15.5 ± 1.3 years) were included in the control group.

2.2. MR imaging

All participants underwent brain MRI twice at an interval of 4 to 6 weeks. MRI scans of the brain were performed using a 3T scanner (MAGNETOM Prisma, Siemens Healthcare, Erlangen, Germany) and a 64-channel head coil. DDE MRI was acquired using a prototype spin-echo echo-planar imaging sequence (TR/TE = 7000 ms/84 ms, diffusion gradient pulse duration time = 12.2 ms, diffusion gradient separation time = 13.7 ms, b-value = 0 and 800 s/mm^2, the number of diffusion directions = 72, voxel size = 1.5 × 1.5 × 4 mm^3, TA = 8:42 min, no slice gap, NEX = 1). T1-weighted 3D MPRAGE sequence (TR/TE/TI = 1900 ms/2.85 ms/900 ms, flip angle = 9°, voxel size = 0.9 × 0.9 × 0.9 mm^3, NEX = 1) was acquired for anatomical information, tissue segmentation, spatial normalization of the reconstructed maps, and calculation of the brain volume. In addition, axial T2-weighted imaging (TR/TE = 4500 ms/87 ms) and FLAIR imaging (TR/TE/TI = 12000 ms/115 ms/2800 ms) were also acquired to exclude gross abnormalities. A review of conventional MR imaging sequences and diffusion images to exclude the abnormalities and artifacts was done by a radiologist with 21-year

experience in neuroimaging.

2.3. Cognitive training

Participants in the training group underwent 30-minute attention network training (ANT) and 30-minute dual N-back training (DBT) for four weeks (60 minutes/day, five days/week) during the interval of MRI acquisition twice. The task performance of ANT and DBT was evaluated on the day of MRI (i.e., before and after the training). Cognitive training was conducted using a notebook computer (resolution 1366 × 768 pixels, refresh rate 60 Hz).

The ANT task is an attention network task (Fan et al., 2002). It was performed in this study using DMDX software (University of Arizona, Tuscon, AZ, USA) (Forster and Forster, 2003). The depiction of the procedure of the ANT task is shown in Figure 1. First, a white fixation cross that has four patterns of presentation time (400 ms, 800 ms, 1200 ms, or 1600 ms) was presented at the screen center. The presentation time was randomly chosen to avoid cue stimulus prediction. After this time interval, one of three cue conditions (i.e. no-cue, center-cue, or spatial-cue) was presented for 100 ms. In the no cue condition, only the fixation cross appeared. In the center-cue condition, a white circular cue stimulus appeared in the same position as the fixation cross. In the spatial-cue condition, a white circular cue stimulus appeared above or below the fixation cross. After a 400 ms interstimulus interval, five white arrows in a row were presented above or below the fixation cross for 1700 ms. The center arrow served as the target stimulus and the other as flanker stimuli. One of two flanker stimuli conditions (i.e. congruent or incongruent) were presented. In the congruent condition, the flanker stimuli appeared in the same direction as the target stimulus. In the incongruent condition, the flanker stimuli appeared in the opposite direction to the target stimulus. The participant was instructed to press the cursor button "→" or "←" on the keyboard to indicate the direction of the target stimulus as fast as possible. The response time (RT) that the participant responded by pressing the cursor button after the appearance of the target stimulus was recorded. The task performance of three subcomponent networks (i.e. alerting, orienting, and executive control) was calculated as $RT_{alerting}$ = RT (no-cue) – RT (center-cue), $RT_{orienting}$ =

RT (center-cue) – RT (spatial-cue), and $RT_{executive\ control}$ = RT (incongruent) – RT (congruent). The RT longer than 1700 ms was considered as an incorrect response. The changes of $RT_{alerting}$, $RT_{orienting}$, and $RT_{executive\ control}$ between the initial and re-assessment were calculated to measure the ANT-derived cognitive improvement.

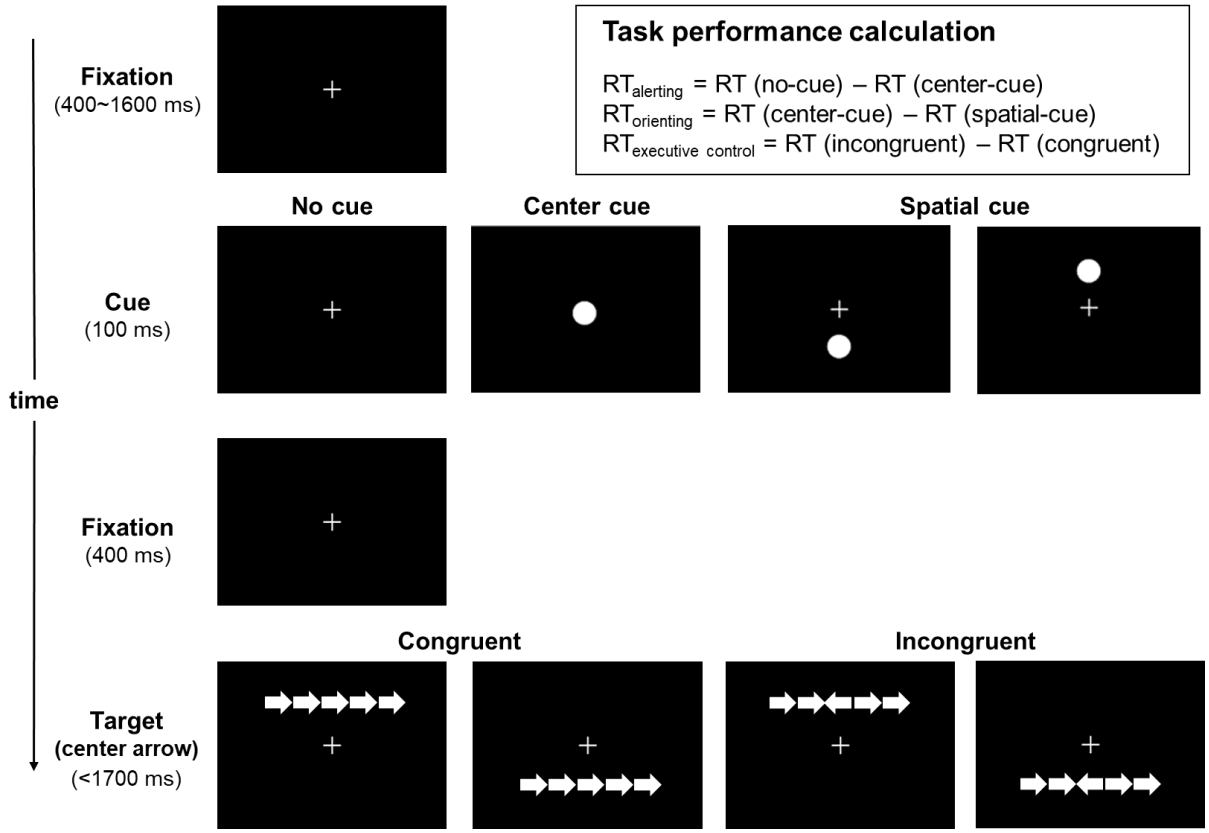

Figure 1. A depiction of the procedure of the attention network training (ANT) task. RT = response time.

The DBT task includes the independent visuospatial and auditory working memory tasks (Jaeggi et al., 2008). The DBT task was built using an in-house JAVA 8 script in this study. The depiction of the procedure of the DBT task is shown in Figure 2. In the visuospatial task, a white 3×3 square was presented on the screen. One of the nine squares was highlighted randomly as the visuospatial stimulus. In the auditory task, randomly selected Japanese phonetic characters, "a", "i", "u", "e", and "o", was simultaneously presented as an auditory stimulus. The stimulus length of visuospatial and auditory stimuli was 500 ms and the interstimulus interval was 2500 ms. The participant was asked to determine whether the current

visuospatial and auditory stimuli were the same as those presented N times before. The training session started with a dual 1-back, and the level of task difficulty (the value of N) was set to increase by one number (e.g., from dual 1-back to dual 2-back) automatically when the participant scored 85% in both tasks for nine consecutive runs. Altogether 600 stimuli were presented in 30 minutes. The task performance was evaluated by error rate, which is the ratio of the number of erroneous responses to the total number of responses to stimuli. The change in error rate between the initial and re-assessment was calculated to measure the DBT-derived cognitive improvement.

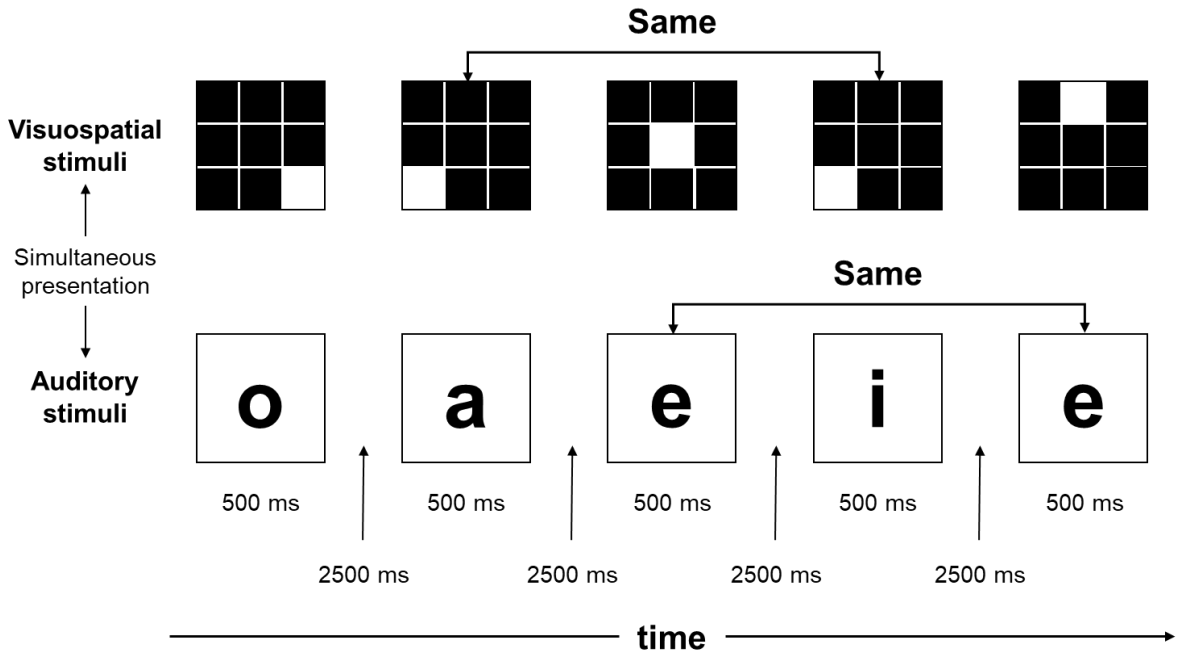

Figure 2. An example of a 2-back condition in the dual N-back training (DBT) task.

2.4. Data processing

From the DDE MRI data, μFA, FA, and MD maps were generated using MATLAB R2009b. μFA was calculated from signal variation between the parallel ($\varphi = 0°$) and orthogonal ($\varphi = 90°$) diffusion gradient pairs, where φ is the angle between the gradient orientations (Yang et al., 2018). Co-registration of reconstructed μFA, FA, and MD maps between the two-time points was performed, followed by co-registration of all these maps to the corresponding MPRAGE images by using the SPM12 software. Next, the MPRAGE images were spatially normalized

to the standard MNI space. The transformation parameters were then applied to the corresponding co-registered μFA, FA, and MD maps. Finally, the normalized μFA, FA, and MD maps were then smoothed with a Gaussian kernel of 3 × 3 × 8 mm FWHM and the normalized MPRAGE images with a Gaussian kernel of 2 × 2 × 2 mm FWHM.

The normalized MPRAGE images of each participant were segmented (SPM12) to calculate the cerebrospinal fluid (CSF) volume, which was considered as a covariate in statistical analyses (MRICron) (Rorden, Karnath, and Bonilha, 2007). The mean normalized MPRAGE images were then generated by averaging the normalized MPRAGE images of all participants (SPM12). A brain parenchyma mask including only the gray and white matter voxels was then formed from the mean normalized MPRAGE images (SPM12), which was further dilated for one voxel to limit partial volume averaging, by using ImageJ (Schneider, Rasband, and Eliceiri, 2012). This mask was applied to all images as an inclusion mask.

2.5. Statistical analysis

A 2 × 2 mixed-design ANOVA was used to evaluate the training and time-related changes of μFA, FA, MD, and GM and WM volumes (SPM12). Age, gender, years of education, and the CSF volume were taken as covariates. Statistical significance was set as uncorrected $P < 0.001$ for clusters containing at least 50 voxels for μFA, FA, and MD, and 10 voxels for GM and WM volumes. The mean values of significant clusters, if any, were extracted (SPM12). The training and time-related changes of the mean RT in the alerting, orienting, and executive control components of ANT and the error rates in DBT were also evaluated using a 2 × 2 mixed-design ANOVA. Statistical significance was also set as uncorrected $P < 0.001$. Changes in the mean μFA, FA, and MD values of the significant clusters between the initial assessment and re-assessment in the training group, if any, were then tested for correlation with changes in RT for components of ANT and the changes in error rate for DBT, using Pearson's product-moment correlation analyses. For this purpose, statistical significance was set as uncorrected $P < 0.05$, and age, gender, years of education, and the CSF volume were taken as covariates. The changes in task performance upon the training and the tests of correlation were performed using SPSS

software version 22.

3. Results

3.1. Cognitive training-derived imaging finding changes

The training and time-related changes in μFA ($F_{(1,27)}$ = 13.54, uncorrected P < 0.001) were observed on 2 × 2 mixed-design ANOVA. Posthoc analyses revealed that the training group had a μFA decrease in the left middle frontal gyrus (uncorrected P < 0.001; 53 voxels; MNI coordinates: X = -36, Y = 54, Z = -6) following the cognitive training. The significant cluster is shown in Figure 3. There were no significant time-related changes in μFA in the control group. Similarly, no significant time-related changes in FA, MD, and the gray and white matter volumes were observed in both groups.

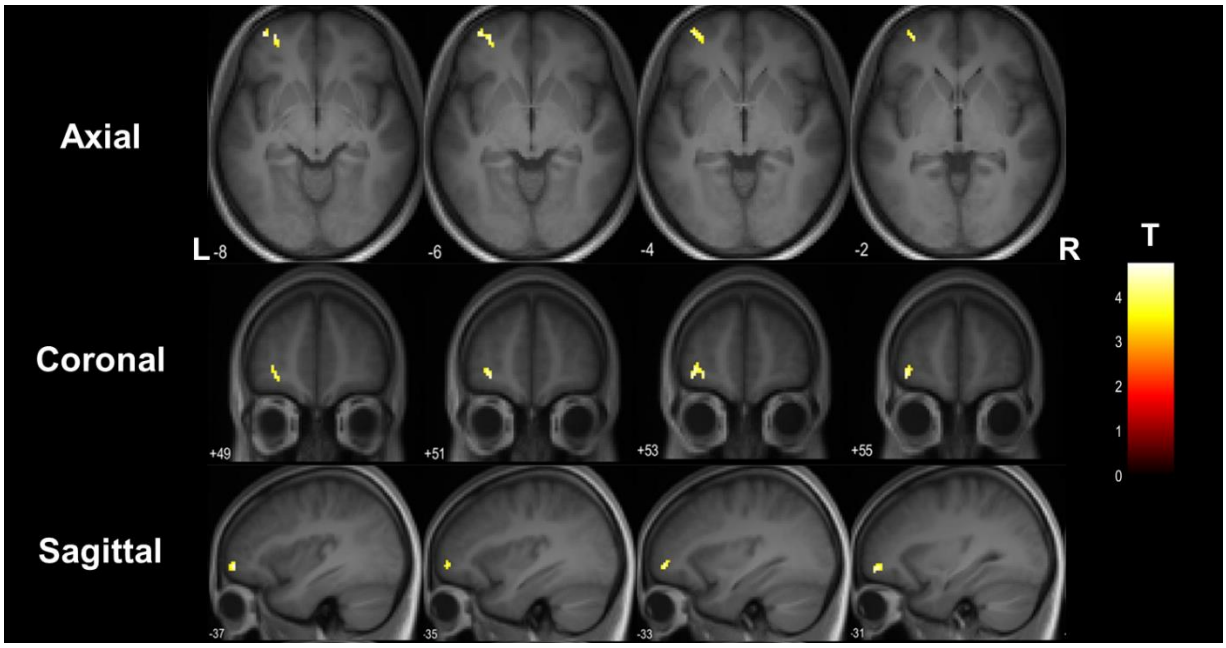

Figure 3. The cluster in the left middle frontal gyrus (MNI coordinates: X=-36, Y=54, Z=-6) showing a decrease in μFA upon the 4-week cognitive training (uncorrected P < 0.001). The cluster is shown as an overlay on axial, coronal, and sagittal 3-dimensional (3D) magnetization prepared rapid acquisition gradient-echo (MPRAGE) template. The look-up table denotes T values. L and R indicate left and right, respectively.

3.2. Cognitive training-derived changes in task performance

The changes in task performance upon cognitive training in ANT and DBT are shown in Figure 4. The 2 × 2 mixed-design ANOVA revealed the training and time-related changes in the RT for the executive control component of ANT ($F_{(1,27)}$ = 8.43, uncorrected P < 0.001) and the error rate in DBT ($F_{(1,27)}$ = 49.59, uncorrected P < 0.001). Posthoc analyses revealed a significant RT decrease in the executive control component of ANT and the DBT error rate in the training group (uncorrected P < 0.001). No significant training and time-related changes were noted in the RT for the alerting and orienting components of ANT in the training group. There were no significant time-related changes in any task performance in the control group.

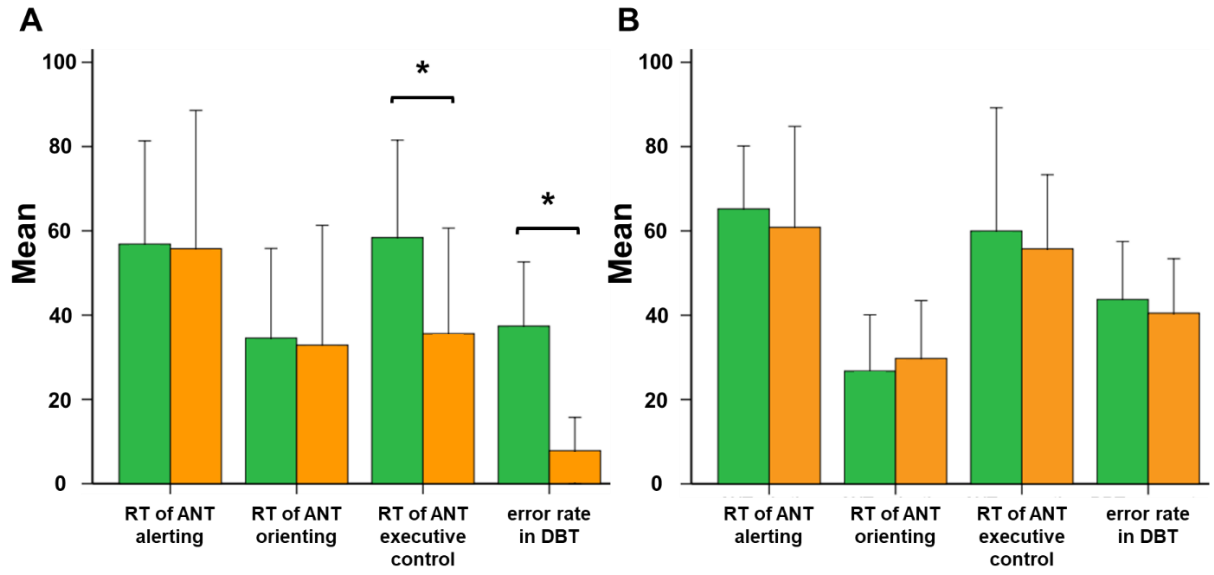

Figure 4. The task performance in response time (RT) of alerting, orienting, and executive control component of attention network training (ANT) and error rate in dual N-back training (DBT) in the (A) training and (B) control groups at initial assessment (green) and re-assessment (orange). The bars and whiskers indicate the mean and standard deviation (SD). * and brackets indicate pairs with statistical significance (uncorrected P < 0.001).

3.3. Relationship between μFA and task performance

The correlations between the change in mean μFA in the left middle frontal gyrus and that of ANT and DBT task performance are shown in Figure 5. There was a significant moderate

negative correlation between the μFA change and the RT change for the orienting component of ANT in the training group (r = -0.521, uncorrected P = 0.032). There were no significant correlations between the μFA change and the RT change for the alerting (r = 0.238, uncorrected P = 0.357) and executive control components (r = -0.223, uncorrected P = 0.389) of ANT and the error rate changes in DBT (r = 0.147, uncorrected P = 0.573) in the training group.

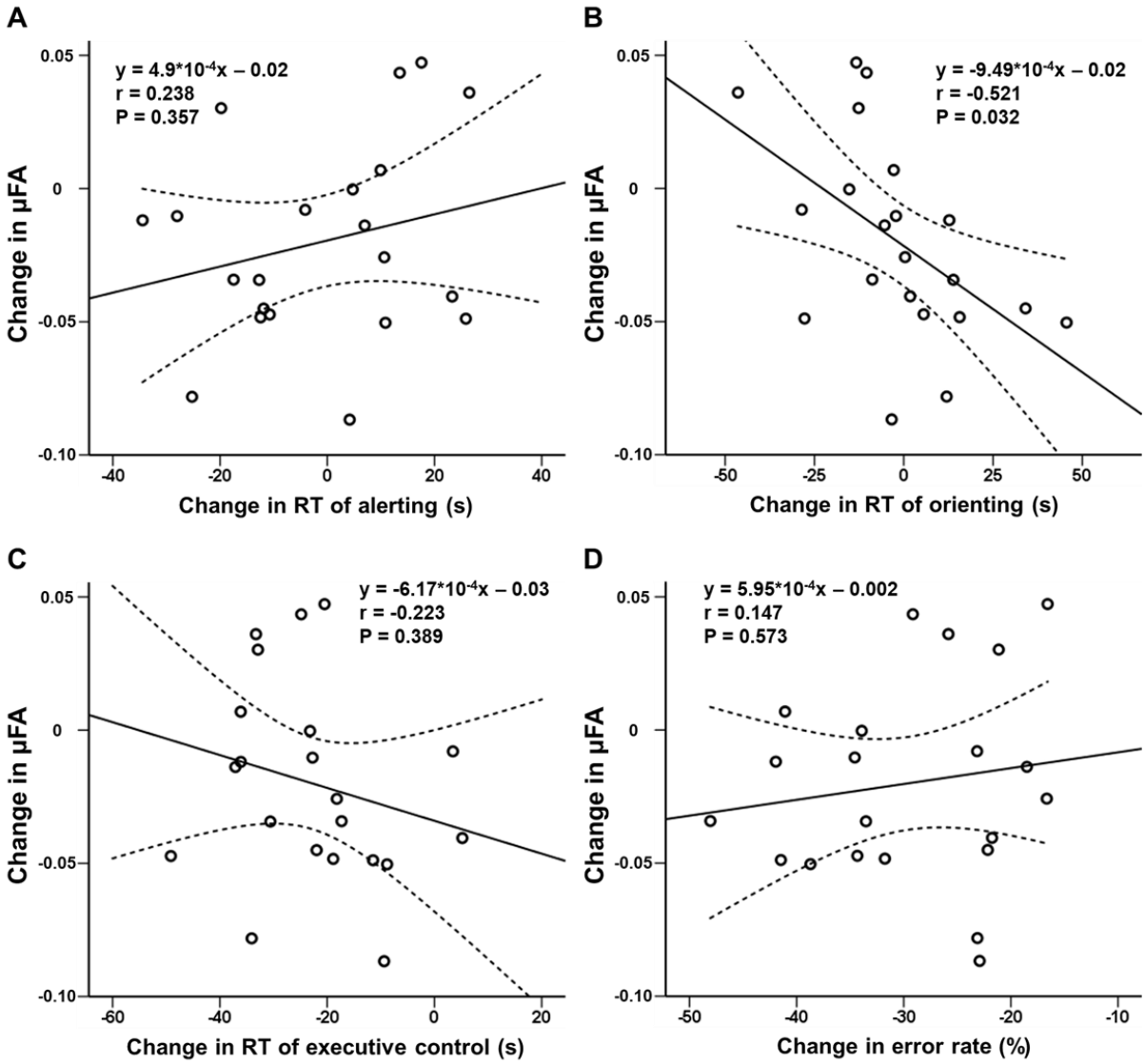

Figure 5. Scatterplots showing correlations in the training group between the μFA change in the left middle frontal gyrus and the response time (RT) changes for the (A) alerting, (B) orienting, and (C) executive control component of attention network training (ANT), and (D) the error rate change in dual N-back training (DBT). The straight and curved lines indicate the

mean and 95% confidence interval.

4. Discussion

In this prospective study, DDE MRI was performed to map the neuroplastic changes following a four-week cognitive training of spatial attention and working memory. To our best knowledge, this is the first report that compared the cognitive training-derived microstructural brain changes among μFA, FA, and MD. The observations of training and time-related change and the correlation with cognitive performance were observed in μFA, but not in the FA and MD, indicating that μFA has higher sensitivity in evaluating cognitive training-derived microstructural changes than FA and MD.

The conventional DTI indices, such as FA and MD, have been used for evaluating the cognitive training-derived microstructural changes in some previous DTI studies in both healthy volunteers as well as patients with neuropsychological disorders (Ghio et al., 2018; Verhelst et al., 2019). In contrast to these previous studies, there were no significant cognitive training-derived microstructural changes in FA and MD in this study. From the location of the observed microstructural change, the DTI indices may not be sensitive enough to detect the change. DTI cannot accurately illustrate the dispersed orientation (multiple intravoxel orientations) of neurites in the gray matter (Shemesh and Cohen, 2011). On the other hand, DDE MRI is designed to solve the problem of orientation dispersion, through its application of two diffusion gradient pairs in two different gradient directions (i.e. parallel and orthogonal directions). By doing so, diffusion signals can be acquired from two different gradient directions which in turn provide more accurate information about tissue microstructure (Szczepankiewicz et al., 2015; Yang et al., 2018). Studies have reported the superior performance of μFA over the DTI indices in detecting trivial brain changes. To list a few, a clinical study observed the differences of μFA in patients with Parkinson's disease and healthy controls, whereas no significant change in FA was observed. In addition, μFA negatively correlated with unified Parkinson's disease rating scale-III scores, but not FA (Ikenouchi et al., 2020). Another clinical study reported improved delineation of multiple sclerosis lesions on

μFA maps, which on the FA maps is confounded by hypointensities caused by crossing fibers (Yang et al., 2018).

The mechanism underlying decreased μFA upon cognitive training may be neuroplasticity, which is the ability of the central nervous system to respond to intrinsic or extrinsic stimuli by modifying its structure, function, and connections (Cramer et al., 2011). Decreased μFA may result from a decrease in neurons or axonal and dendritic synapses, which may reflect synaptic pruning. Synaptic pruning is a neuroplastic process, which facilitates changes in the neural structures by reducing the overall number of neurons and synapses, leaving more efficient synaptic configurations (Laughlin and Sejnowski, 2003). In this study, no volumetric changes were observed upon cognitive training, suggestive of the higher sensitivity of μFA changes than volumetric changes in detecting neuroplastic changes.

Regarding the ANT and DBT task performance, significant decreases in RT in the executive control component of ANT and the DBT error rate were observed upon cognitive training, suggestive of improved task performance in executive and working memory function. Task performance of executive control was evaluated by subtracting RT between incongruent and congruent conditions. Because the RT was relatively stable for the congruent condition, changes in RT in the performance of executive control are considered as mainly influenced by the RT in the incongruent condition. The results further indicate that the participants were less affected by flanker stimuli on response selection and could identify the target stimulus faster upon the training. These observations are in accord with several previous studies, which showed improved task performance of executive control in ANT and working memory in DBT upon cognitive training (Rueda, Checa, and Cómbita, 2012; Salminen, Strobach, and Schubert, 2012). In this study, a moderate negative correlation was observed between the μFA change in the left middle frontal gyrus and the RT change for the orienting component of ANT. The middle frontal gyrus is known to modulate attention. There has been fMRI evidence about the role of the middle frontal gyrus in reorienting visuospatial attention. Higher fMRI activation in bilateral middle frontal gyri has been observed in the invalid cue condition (i.e. the target appeared on the opposite side) than the valid cue condition (i.e. the target appeared on the same

side) in healthy volunteers who undertook cued target detection tasks (Thiel, Zilles, and Fink, 2004). It is thus believed that improved task performance is the consequence of cognitive training-derived neuroplastic changes.

Several limitations need to be addressed. First, considering that this is an exploratory study, correction for multiple testing was not performed in tests of correlation. Ideally, this should be done. Second, handedness was not evaluated so that whether it had affected the results is not known. In an fMRI study, right-handers were found to have leftward lateralization in visuospatial attention-related activations in the middle frontal gyrus, and vice versa (Petit et al., 2015). Third, several newer single diffusion encoding techniques such as diffusion kurtosis imaging and neurite orientation density and dispersion imaging have been reported as can evaluate microstructural brain changes (Jensen et al., 2005; Zhang et al., 2012). This study did not compare the performance of DDE MRI to these techniques. Finally, the results of this study suggest the usefulness of μFA in revealing cognitive training-derived microstructural changes, it is not known how long these microstructural changes would last. This is beyond the scope of this study. A longitudinal study may provide an answer to this question.

5. Conclusion

Cognitive training-derived μFA changes, but not FA and MD, were observed, suggesting that μFA is suited to evaluate these changes. The correlation of μFA changes with orienting task performance was observed in the left middle frontal gyrus that modules attention, suggesting that μFA can become a sensitive marker to evaluate cognitive training-derived improved attention.

Summary and conclusions

In this study, the brain microstructure was explored by using DSI and DDE MRI. The summary of findings are as follows:

1) Widespread regional variations in GFA, NQA, FA, and MD were observed across the whole brain. Women had lower GFA, higher FA, and higher MD in several anatomical locations than men. Age-dependent decrease in GFA, NQA, and FA was observed in the majority of anatomical locations.

2) NAA/Cr and MD have similar and reverse patterns of lateralization of GFA, NQA, and FA. Cho/Cr, Glx/Cr, and mI/Cr were independent of lateralization of GFA, NQA, and FA. Combined evaluation with neurometabolites has provided more complete information about the composition of neural architecture.

3) After 4-week attention and working memory training, the microstructural changes were observed in μFA, but not in FA and MD. The correlation of μFA changes with orienting task performance of ANT was observed in the left middle frontal gyrus that plays an important role in the modulation of attention.

In chapters 1 and 2, the normative values in DSI indices were measured and variations of these indices in anatomical location, side, gender, and age, and the association with neurometabolites in hemispheric lateralization were evaluated. These normative values in DSI indices are considered as helpful for the interpretation of pathological states in further whole-brain clinical studies. In chapter 3, cognitive training and time-related μFA changes in the left middle frontal gyrus and the correlation between μFA with attentional performance were observed, but not FA, indicating that μFA is more sensitive than FA in evaluating cognitive training-derived improved attention. From these findings, DDE MRI and μFA are thought to be useful in the further evaluation of the brain in clinical psychological studies.

Acknowledgment

This study was partly funded by the Grant-in-Aid for Scientific Research by Japanese Society for Promotion of Science (15K01358, 24591741, and 19K11317) and the Global Institution for Collaborative Research and Education, Hokkaido University. This paper is a summary of the research results obtained under the guidance of Associate Professor Khin Khin Tha from the Department of Biomarker Imaging Science, Graduate School of Biomedical Science and Engineering, Hokkaido University.

First, I would like to express my great appreciation to Associate Professor Khin Khin Tha who kindly accepted me as a doctoral course student to study at the Department of Biomarker Imaging Science, Graduate School of Biomedical Science and Engineering, and painlessly guided me in every step involved in this thesis work. Thanks to her excellent guidance, I had a wonderful time while undertaking my doctoral program.

Second, I would also like to express my great appreciation to Assistant Professor Ryusuke Suzuki, at the Graduate School of Medical Science and Engineering, Hokkaido University, for kindly guiding me to promote my study smoothly.

Third, I would also like to express my sincere gratitude to Professor Hiroki Shirato for giving me some beneficial guidance for the study, Lecturer Mr. Daisuke Sawamura and clinical technician Mr. Hiroyuki Hamaguchi as the same members belongs to doctoral courses at the Department of Biomarker Imaging Science, for their help with the MRI scans and many useful advices for data analyses, Mr. Yuta Urushibata for his help with kind guidance for data analyses, Ms. Machiko Kishi and Ms. Sonoe Takayama for helping me with the paper works involved during the doctoral course, and all participants in this study who kindly volunteered for MRI.

Finally, I also want to express my deep appreciation to my parents who always support and encourage me to study abroad in Japan.

Reference

Amunts, K., Schlaug, G., Schleicher, A., Steinmetz, H., Dabringhaus, A., Roland, P.E., Zilles, K. (1996). Asymmetry in the human motor cortex and handedness. Neuroimage 4, 216-222.

Alexander, M. P., Naeser, M. A., Palumbo, C. (1990). Broca's area aphasias: aphasia after lesions including the frontal operculum. Neurology 40, 353-362.

Basser, P.J., Pierpaoli, C. (1996). Microstructural and physiological features of tissues elucidated by quantitative-diffusion-tensor MRI. J. Magn. Reson. B. 111, 209-219.

Bhagat, Y.A., Beaulieu, C. (2004). Diffusion anisotropy in subcortical white matter and cortical gray matter: changes with aging and the role of CSF-suppression. J. Magn. Reson. Imaging 20, 216-227.

Bilgic, B., Setsompop, K., Cohen-Adad, J., Wedeen, V., Wald, L. L., Adalsteinsson, E. (2012). Accelerated diffusion spectrum imaging with compressed sensing using adaptive dictionaries. Med. Image Comput. Comput. Assist. Interv. 15, 1-9.

Birch, R., Peet, A.C., Dehghani, H., Wilson, M. (2017). Influence of macromolecule baseline on ^{1}H MR spectroscopic imaging reproducibility. Magn. Reson. Med. 77, 34-43.

Bjartmar, C., Battistuta, J., Terada, N., Dupree, E., Trapp, B.D. (2002). N-acetylaspartate is an axon-specific marker of mature white matter in vivo: a biochemical and immunohistochemical study on the rat optic nerve. Ann. Neurol. 51, 51-58.

Blumenfeld-Katzir, T., Pasternak, O., Dagan, M., Assaf, Y. (2011). Diffusion MRI of structural brain plasticity induced by a learning and memory task. PLoS ONE 6, e20678.

Bowley, M.P., Cabral, H., Rosene, D.L., Peters, A. (2010). Age changes in myelinated nerve fibers of the cingulate bundle and corpus callosum in the rhesus monkey. J. Comp. Neurol. 518, 3046-3064.

Brander, A., Kataja, A., Saastamoinen, A., Ryymin, P., Huhtala, H., Ohman, J., Soimakallio, S., Dastidar, P. (2010). Diffusion tensor imaging of the brain in a healthy adult population: Normative values and measurement reproducibility at 3 T and 1.5 T. Acta. Radiol. 51, 800-807.

Budde, M. D., Janes, L., Gold, E., Turtzo, L. C., Frank, J. A. (2011). The contribution of gliosis to diffusion tensor anisotropy and tractography following traumatic brain injury: validation in the rat using Fourier analysis of stained tissue sections. Brain 134, 2248-2260.

Chiu, C.H., Lo, Y.C., Tang, H.S., Liu, I.C., Chiang, W.Y., Yeh, F.C., Jaw, F.S., Tseng, W.Y. (2011). White matter abnormalities of fronto-striato-thalamic circuitry in obsessive-compulsive disorder: A study using diffusion spectrum imaging tractography. Psychiatry Res. 192, 176-182.

Coghill, R. C., Gilron, I., Iadarola, M. J. (2001). Hemispheric lateralization of somatosensory processing. J. Neurophysiol. 85, 2602-2612.

Compston, A., Zajicek, J., Sussman, J., Webb, A., Hall, G., Muir, D., Shaw, C., Wood, A., Scolding, N. (1997). Glial lineages and myelination in the central nervous system. J. Anat. 190, 161-200.

Cramer, S.C., Sur, M., Dobkin, B.H., O'Brien, C., Sanger, T.D., Trojanowski, J.Q., Rumsey, J.M., Hicks, R., Cameron, J., Chen, D., et al. (2011). Harnessing neuroplasticity for clinical applications. Brain 134, 1591–1609.

Crespi, C., Laureiro-Martínez, D., Dodich, A., Cappa, S.F., Brusoni, S., Zollo, M., Falini, A., Canessa, N. (2018). Improving innovative decision-making: Training-induced changes in fronto-parietal networks. Brain Cogn. 128, 46-55.

Uylings, H.B., Jacobsen, A.M., Zilles, K., Amunts, K. (2006). Left-right asymmetry in volume and number of neurons in adult Broca's area. Cortex 42, 652-658.

Das, S.K., Wang, J.L., Bing, L., Bhetuwal, A., Yang, H.F. (2017). Regional Values of Diffusional Kurtosis Estimates in the Healthy Brain during Normal Aging. Clin. Neuroradiol. 27, 283-298.

Ding, X.Q., Maudsley, A.A., Sabati, M., Sheriff, S., Dellani, P.R., Lanfermann, H. (2015). Reproducibility and reliability of short-TE whole-brain MR spectroscopic imaging of human brain at 3T. Magn. Reson. Med. 73, 921-928.

Faizy, T.D., Thaler, C., Broocks, G., Flottmann, F., Leischner, H., Kniep, H., Nawabi, J., Schön, G., Stellmann, J.P., Kemmling, A., et al. (2020). The Myelin Water Fraction Serves as a Marker

for Age-Related Myelin Alterations in the Cerebral White Matter - A Multiparametric MRI Aging Study. Front. Neurosci. 14, 136.

Fan, J., McCandliss, B.D., Sommer, T., Raz, A., Posner, M.I. (2002). Testing the efficiency and independence of attentional networks. J. Cogn. Neurosci. 14, 340-347.

Faul, F., Erdfelder, E., Buchner, A., Lang, A.G. (2009). Statistical power analyses using G*Power 3.1: tests for correlation and regression analyses. Behav. Res. Methods 41, 1149-1160.

Fernández-Miranda, J.C., Wang, Y., Pathak, S., Stefaneau, L., Verstynen, T., Yeh, F.C. (2015). Asymmetry, connectivity, and segmentation of the arcuate fascicle in the human brain. Brain Struct. Funct. 220, 1665-1680.

Forster, K.I., Forster, J.C. (2003). DMDX: a Windows display program with millisecond accuracy. Behav. Res. Methods Instrum. Comput. 35, 116-124.

Friedrich, P., Fraenz, C., Schlüter, C., Ocklenburg, S., Mädler, B., Güntürkün, O., Genç, E. (2020). The Relationship Between Axon Density, Myelination, and Fractional Anisotropy in the Human Corpus Callosum. Cereb. Cortex 30, 2042-2056.

Fujiyoshi, K., Konomi, T., Yamada, M., Hikishima, K., Tsuji, O., Komaki, Y., Okano, H. (2013). Diffusion tensor imaging and tractography of the spinal cord: from experimental studies to clinical application. Exp. Neurol. 242, 74-82.

Ghio, M., Locatelli, M., Tettamanti, A., Perani, D., Gatti, R., Tettamanti, M. (2018). Cognitive training with action-related verbs induces neural plasticity in the action representation system as assessed by gray matter brain morphometry. Neuropsychologia 114, 186-194.

Glenn, G.R., Kuo, L.W., Chao, Y.P., Lee, C.Y., Helpern, J.A., Jensen, J.H. (2016). Mapping the Orientation of White Matter Fiber Bundles: A Comparative Study of Diffusion Tensor Imaging, Diffusional Kurtosis Imaging, and Diffusion Spectrum Imaging. AJNR. Am. J. Neuroradiol. 37, 1216-1222.

Highley, J.R., Walker, M.A., Esiri, M.M., Crow, T.J., Harrison, P.J. (2002). Asymmetry of the uncinate fasciculus: a post-mortem study of normal subjects and patients with schizophrenia. Cereb. Cortex 12, 1218-1224.

Huster, R.J., Westerhausen, R., Kreuder, F., Schweiger, E., Wittling, W. (2009). Hemispheric

and gender related differences in the midcingulum bundle: a DTI study. Hum. Brain Mapp. 30, 383-391.

Ikenouchi, Y., Kamagata, K., Andica, C., Hatano, T., Ogawa, T., Takeshige-Amano, H., Kamiya, K., Wada, A., Suzuki, M., Fujita, S., et al. (2020). Evaluation of white matter microstructure in patients with Parkinson's disease using microscopic fractional anisotropy. Neuroradiology 62, 197-203.

Jack, C.R., Jr, Twomey, C.K., Zinsmeister, A.R., Sharbrough, F.W., Petersen, R.C., Cascino, G.D. (1989). Anterior temporal lobes and hippocampal formations: normative volumetric measurements from MR images in young adults. Radiology 172, 549-554.

Jaeggi, S.M., Buschkuehl, M., Jonides, J., Perrig, W.J. (2008). Improving fluid intelligence with training on working memory. Proc. Natl. Acad. Sci. U. S. A. 105, 6829-6833.

Jensen, J.H., Helpern, J.A., Ramani, A., Lu, H., Kaczynski, K. (2005). Diffusional kurtosis imaging: the quantification of non-gaussian water diffusion by means of magnetic resonance imaging. Magn. Reson. Med. 53, 1432-1440.

Kamiya, K., Kamagata, K., Ogaki, K., Hatano, T., Ogawa, T., Takeshige-Amano, H., Murata, S., Andica, C., Murata, K., Feiweier, T., et al. (2020). Brain White-Matter Degeneration Due to Aging and Parkinson Disease as Revealed by Double Diffusion Encoding. Front. Neurosci. 14, 584510.

Kimura, D. (1996). Sex, sexual orientation and sex hormones influence human cognitive function. Curr. Opin. Neurobiol. 6, 259–263.

Kono, K., Inoue, Y., Nakayama, K., Shakudo, M., Morino, M., Ohata, K., Wakasa, K., Yamada, R. (2001). The role of diffusion-weighted imaging in patients with brain tumors. AJNR. Am. J. Neuroradiol. 22, 1081-1088.

Kuo, L. W., Chen, J. H., Wedeen, V. J., Tseng, W. Y. (2008). Optimization of diffusion spectrum imaging and q-ball imaging on clinical MRI system. Neuroimage 41, 7-18.

Lampit, A., Hallock, H., Suo, C., Naismith, S. L., Valenzuela, M. (2015). Cognitive training-induced short-term functional and long-term structural plastic change is related to gains in global cognition in healthy older adults: a pilot study. Front. Aging Neurosci. 7, 14.

Lansberg, M.G., Norbash, A.M., Marks, M.P., Tong, D.C., Moseley, M.E., Albers, G.W. (2000). Advantages of adding diffusion-weighted magnetic resonance imaging to conventional magnetic resonance imaging for evaluating acute stroke. Arch. Neurol. 57, 1311-1316.

Lasič, S., Szczepankiewicz, F., Eriksson, S., Nilsson, M., Topgaard, D. (2014). Microanisotropy imaging: quantification of microscopic diffusion anisotropy and orientational order parameter by diffusion MRI with magic-angle spinning of the q-vector. Front. Phys. 2, 11.

Lätt, J., Nilsson, M., Wirestam, R., Ståhlberg, F., Karlsson, N., Johansson, M., Sundgren, P.C., van Westen, D. (2013). Regional values of diffusional kurtosis estimates in the healthy brain. J. Magn. Reson. Imaging 37, 610-618.

Laughlin, S.B., Sejnowski, T.J. (2003). Communication in neuronal networks. Science 301, 1870-1874.

Lee, C. E., Danielian, L. E., Thomasson, D., Baker, E. H. (2009). Normal regional fractional anisotropy and apparent diffusion coefficient of the brain measured on a 3 T MR scanner. Neuroradiology 51, 3-9.

Leuthardt, E.C., Wippold, F.J., Oswood, M.C., Rich, K.M. (2002). Diffusion-weighted MR imaging in the preoperative assessment of brain abscesses. Surg. Neurol. 58, 395-402.

Liu, X., Gao, X., Zhang, L., Yuan, Z., Zhang, C., Lu, W., Cui, D., Zheng, F., Qiu, J., Xie, J. (2018). Age-related changes in fiber tracts in healthy adult brains: A generalized q-sampling and connectometry study. J. Magn. Reson. Imaging 48, 369-381.

Maldjian, J. A., Laurienti, P. J., Kraft, R. A., Burdette, J. H. (2003). An automated method for neuroanatomic and cytoarchitectonic atlas-based interrogation of fMRI data sets. Neuroimage 19, 1233-1239.

Maraganore, D. M., Folger, W. N., Swanson, J. W., Ahlskog, J. E. (1992). Movement disorders as sequelae of central pontine myelinolysis: report of three cases. Mov. Disord. 7:142-148.

Maudsley, A.A., Domenig, C., Govind, V., Darkazanli, A., Studholme, C., Arheart, K., Bloomer, C. (2009). Mapping of brain metabolite distributions by volumetric proton MR spectroscopic imaging (MRSI). Magn. Reson. Med. 61, 548-559.

Maudsley, A. A., Roy, B., Gupta, R. K., Sheriff, S., Awasthi, R., Gu, M., Husain, N., Mohakud, S., Behari, S., Spielman, D. M. (2014). Association of metabolite concentrations and water diffusivity in normal appearing brain tissue with glioma grade. J. Neuroimaging 24:585-589.

Maudsley, A.A., Govind, V., Saigal, G., Gold, S.G., Harris, L., Sheriff, S. (2017). Longitudinal MR Spectroscopy Shows Altered Metabolism in Traumatic Brain Injury. J. Neuroimaging 27, 562-569.

Meier-Ruge, W., Ulrich, J., Brühlmann, M., Meier, E. (1992). Age-related white matter atrophy in the human brain. Ann. N. Y. Acad. Sci. 673, 260-269.

Menzler, K., Belke, M., Wehrmann, E., Krakow, K., Lengler, U., Jansen, A., Hamer, H. M., Oertel, W. H., Rosenow, F., Knake, S. (2011). Men and women are different: diffusion tensor imaging reveals sexual dimorphism in the microstructure of the thalamus, corpus callosum and cingulum. Neuroimage 54, 2557-2562.

Mitra, P.P. (1995). Multiple wave-vector extensions of the NMR pulsed-field-gradient spin-echo diffusion measurement. Phys. Rev. B. Condens. Matter 51, 15074-15078.

Nitta, N., Shiino, A., Watanabe, T., Sakaue, Y., Nozaki, K. (2012). Buccofacial apraxia without limb apraxia or aphasia after right premotor area contusion: a case report. No Shinkei Geka 40, 985-990.

Oldfield, R.C. (1971). The assessment and analysis of handedness: the Edinburgh inventory. Neuropsychologia 9, 97-113.

Orimo, H. (2006). Reviewing the definition of elderly. Nihon Ronen Igakkai Zasshi. 43, 27-34.

Oshida, K., Shimizu, T., Takase, M., Tamura, Y., Shimizu, T., Yamashiro, Y. (2003). Effects of dietary sphingomyelin on central nervous system myelination in developing rats. Pediatr. Res. 53, 589-593.

Owen, A. M., Stern, C. E., Look, R. B., Tracey, I., Rosen, B. R., Petrides, M. (1998). Functional organization of spatial and nonspatial working memory processing within the human lateral frontal cortex. Proc. Natl. Acad. Sci. U. S. A. 95, 7721-7726.

Ozarslan, E. (2009). Compartment shape anisotropy (CSA) revealed by double pulsed field gradient MR. J. Magn. Reson. 199, 56-67.

Panesar, S.S., Yeh, F.C., Deibert, C.P., Fernandes-Cabral, D., Rowthu, V., Celtikci, P., Celtikci, E., Hula, W.D., Pathak, S., Fernández-Miranda, J.C. (2017). A diffusion spectrum imaging-based tractographic study into the anatomical subdivision and cortical connectivity of the ventral external capsule: uncinate and inferior fronto-occipital fascicles. Neuroradiology 59, 971-987.

Park, H.J., Westin, C.F., Kubicki, M., Maier, S.E., Niznikiewicz, M., Baer, A., Frumin, M., Kikinis, R., Jolesz, F.A., McCarley, R.W., et al. (2004). White matter hemisphere asymmetries in healthy subjects and in schizophrenia: a diffusion tensor MRI study. Neuroimage 1, 213-223.

Petit, L., Zago, L., Mellet, E., Jobard, G., Crivello, F., Joliot, M., Mazoyer, B., Tzourio-Mazoyer, N. (2015). Strong rightward lateralization of the dorsal attentional network in left-handers with right sighting-eye: an evolutionary advantage. Hum. Brain Mapp. 36, 1151-1164.

Pierpaoli, C., Basser, P.J. (1996). Toward a quantitative assessment of diffusion anisotropy. Magn. Reson. Med. 36, 893-906.

Pouwels, P.J., Frahm, J. (1998). Regional metabolite concentrations in human brain as determined by quantitative localized proton MRS. Magn. Reson. Med. 39, 53-60.

Rebok, G.W., Ball, K., Guey, L.T., Jones, R.N., Kim, H.Y., King, J.W., Marsiske, M., Morris, J.N., Tennstedt, S.L., Unverzagt, F.W., et al. (2014). Ten-year effects of the advanced cognitive training for independent and vital elderly cognitive training trial on cognition and everyday functioning in older adults. J. Am. Geriatr. Soc. 62, 16-24.

Rochefort, C., Lefort, J. M., Rondi-Reig, L. (2013). The cerebellum: a new key structure in the navigation system. Front. Neural Circuits 7, 35.

Rorden, C., Karnath, H.O., Bonilha, L. (2007). Improving lesion-symptom mapping. J. Cogn. Neurosci. 19, 1081-1088.

Rueda, M. R., Checa, P., Cómbita, L. M. (2012). Enhanced efficiency of the executive attention network after training in preschool children: immediate changes and effects after two months. Dev. Cogn. Neurosci. 2 Suppl 1(Suppl 1), S192–S204.

Salminen, T., Strobach, T., Schubert, T. (2012). On the impacts of working memory training on executive functioning. Front. Hum. Neurosci. 6, 166.

Sandell, J.H., Peters, A. (2003). Disrupted myelin and axon loss in the anterior commissure of the aged rhesus monkey. J. Comp. Neurol. 466, 14-30.

Schneider, C.A., Rasband, W.S., Eliceiri, K.W. (2012). NIH Image to ImageJ: 25 years of image analysis. Nat. Methods. 9, 671-675.

Shemesh, N., Cohen, Y. (2011). Microscopic and compartment shape anisotropies in gray and white matter revealed by angular bipolar double-PFG MR. Magn. Reson. Med. 65, 1216-1227.

Sun, T., Walsh, C.A. (2006). Molecular approaches to brain asymmetry and handedness. Nat. Rev. Neurosci. 7, 655-662.

Szczepankiewicz, F., Lasič, S., van Westen, D., Sundgren, P.C., Englund, E., Westin, C.F., Ståhlberg, F., Lätt, J., Topgaard, D., Nilsson, M. (2015). Quantification of microscopic diffusion anisotropy disentangles effects of orientation dispersion from microstructure: applications in healthy volunteers and in brain tumors. Neuroimage 104, 241-252.

Takao, H., Abe, O., Yamasue, H., Aoki, S., Sasaki, H., Kasai, K., Yoshioka, N., Ohtomo, K. (2011). Gray and white matter asymmetries in healthy individuals aged 21-29 years: a voxel-based morphometry and diffusion tensor imaging study. Hum. Brain Mapp. 10, 1762-1773.

Takao, H., Hayashi, N., Ohtomo, K. (2014). Sex dimorphism in the white matter: fractional anisotropy and brain size. J. Magn. Reson. Imaging 39, 917-923.

Teipel, S.J., Lerche, M., Kilimann, I., O'Brien, K., Grothe, M., Meyer, P., Li, X., Sänger, P., Hauenstein, K. (2014). Decline of fiber tract integrity over the adult age range: a diffusion spectrum imaging study. J. Magn. Reson. Imaging 40, 348-359.

Terry, R. D., DeTeresa, R., Hansen, L. A. (1987). Neocortical cell counts in normal human adult aging. Ann. Neurol. 21, 530-539.

Tha, K.K., Terae, S., Yabe, I., Miyamoto, T., Soma, H., Zaitsu, Y., Fujima, N., Kudo, K., Sasaki, H., Shirato, H. (2010). Microstructural white matter abnormalities of multiple system atrophy: in vivo topographic illustration by using diffusion-tensor MR imaging. Radiology 255, 563-569.

Tha, K.K., Terae, S., Nakagawa, S., Inoue, T., Kitagawa, N., Kako, Y., Nakato, Y., Akter Popy, K., Fujima, N., Zaitsu, Y., et al. (2013). Impaired integrity of the brain parenchyma in non-

geriatric patients with major depressive disorder revealed by diffusion tensor imaging. Psychiatry Res. 212, 208-215.

Thiebaut de Schotten, M., Ffytche, D.H., Bizzi, A., Dell'Acqua, F., Allin, M., Walshe, M., Murray, R., Williams, S.C., Murphy, D.G., Catani, M. (2011). Atlasing location, asymmetry and inter-subject variability of white matter tracts in the human brain with MR diffusion tractography. Neuroimage 54, 49-59.

Thiel, C.M., Zilles, K., Fink, G.R. (2004). Cerebral correlates of alerting, orienting and reorienting of visuospatial attention: an event-related fMRI study. Neuroimage 21, 318-328.

Tuch, D.S. (2004). Q-ball imaging. Magn. Reson. Med. 52, 1358-1372.

Turkeltaub, P.E., Coslett, H.B. (2010). Localization of sublexical speech perception components. Brain Lang. 114, 1-15.

Uylings, H.B.M., Jacobsen, A.M., Zilles, K., Amunts, K. (2006). Left-Right Asymmetry in Volume and Number of Neurons in Adult Broca's Area. Cortex 42, 652-658.

Van Paesschen, W., Connelly, A., King, M.D., Jackson, G.D., Duncan, J.S. (1997). The spectrum of hippocampal sclerosis: a quantitative magnetic resonance imaging study. Ann. Neurol. 41, 41-51.

Verhelst, H., Giraldo, D., Vander Linden, C., Vingerhoets, G., Jeurissen, B., Caeyenberghs, K. (2019). Cognitive Training in Young Patients With Traumatic Brain Injury: A Fixel-Based Analysis. Neurorehabil. Neural Repair 33, 813-824.

Wakana, S., Caprihan, A., Panzenboeck, M.M., Fallon, J.H., Perry, M., Gollub, R.L., Hua, K., Zhang, J., Jiang, H., Dubey, P., et al. (2007). Reproducibility of quantitative tractography methods applied to cerebral white matter. Neuroimage 36, 630-644.

Wang, Z.M., Wei, P.H., Shan, Y., Han, M., Zhang, M., Liu, H., Gao, J.H., Lu, J. (2020). Identifying and characterizing projections from the subthalamic nucleus to the cerebellum in humans. Neuroimage 210, 116573.

Wedeen, V. J., Hagmann, P., Tseng, W. Y., Reese, T. G., Weisskoff, R. M. (2005). Mapping complex tissue architecture with diffusion spectrum magnetic resonance imaging. Magn. Reson. Med. 54, 1377-1386.

Wedeen, V.J., Wang, R.P., Schmahmann, J.D., Benner, T., Tseng, W.Y., Dai, G., Pandya, D.N., Hagmann, P., D'Arceuil, H., de Crespigny, A.J. (2008). Diffusion spectrum magnetic resonance imaging (DSI) tractography of crossing fibers. Neuroimage 41, 1267-1277.

Yang, G., Tian, Q., Leuze, C., Wintermark, M., McNab, J.A. (2018). Double diffusion encoding MRI for the clinic. Magn. Reson. Med. 80, 507-520.

Yeh, F.C., Wedeen, V.J., Tseng, W.Y. (2010). Generalized q-sampling imaging. IEEE. Trans. Med. Imaging 29, 1626-1635.

Zhang, H., Schneider, T., Wheeler-Kingshott, C.A., Alexander, D.C. (2012). NODDI: practical in vivo neurite orientation dispersion and density imaging of the human brain. Neuroimage 61, 1000-1016.

Zhang, Y., Taub, E., Salibi, N., Uswatte, G., Maudsley, A.A., Sheriff, S., Womble, B., Mark, V.W., Knight, D.C. (2018). Comparison of reproducibility of single voxel spectroscopy and whole-brain magnetic resonance spectroscopy imaging at 3T. NMR. Biomed. 31, e3898.